The isotopic composition of near-surface water vapor at the Maïdo observatory (Reunion Island, southwestern Indian Ocean) documents the controls of the humidity of the subtropical troposphere

Etienne Guilpart, Françoise Vimeux, Stéphanie Evan, Jérôme Brioude, Jean-Marc Metzger, Christelle Barthe, Camille Risi, Olivier Cattani

AGU PUBLICATIONS

JGR

Journal of Geophysical Research: Atmospheres

RESEARCH ARTICLE
10.1002/2017JD026791

Key Point:
- Humidity measurements in Reunion Island are tracers of moisture variability; water stable isotopes reveal the controls on this variability

Supporting Information:
- Supporting Information S1

Correspondence to:
E. Guilpart and F. Vimeux,
etienne.guilpart@lsce.ipsl.fr;
francoise.vimeux@lsce.ipsl.fr

Citation:
Guilpart, E., F. Vimeux, S. Evan, J. Brioude, J.-M. Metzger, C. Barthe, C. Risi, and O. Cattani (2017), The isotopic composition of near-surface water vapor at the Maïdo observatory (Reunion Island, southwestern Indian Ocean) documents the controls of the humidity of the subtropical troposphere, *J. Geophys. Res. Atmos.*, *122*, 9628–9650, doi:10.1002/2017JD026791.

Received 13 MAR 2017
Accepted 24 AUG 2017
Accepted article online 29 AUG 2017
Published online 22 SEP 2017

The isotopic composition of near-surface water vapor at the Maïdo observatory (Reunion Island, southwestern Indian Ocean) documents the controls of the humidity of the subtropical troposphere

Etienne Guilpart[1], Françoise Vimeux[1,2], Stéphanie Evan[3], Jérôme Brioude[3], Jean-Marc Metzger[4], Christelle Barthe[3], Camille Risi[5], and Olivier Cattani[2]

[1]Laboratoire des Sciences du Climat et de l'Environnement, IPSL, UMR 8212 (CEA, CNRS, UVSQ), Gif-sur-Yvette, France, [2]Institut de Recherche pour le Développement, Laboratoire HydroSciences Montpellier, UMR 5569 (CNRS, IRD, UM), Montpellier, France, [3]Laboratoire de l'Atmosphère et des Cyclones, UMR 8105 (CNRS, Université de La Réunion, Météo-France), Saint-Denis de La Réunion, France, [4]Observatoire des Sciences de l'Univers de la Réunion, UMS 3365 (CNRS, Université de La Réunion), Saint-Denis de La Réunion, France, [5]Laboratoire de Météorologie Dynamique, IPSL, Sorbonne Universités, UMR 8539 (CNRS, ENS, X, UPMC), Paris, France

Abstract We present a 1 year long record of the isotopic composition of near-surface water vapor ($\delta^{18}O_v$) at the Maïdo atmospheric observatory (Reunion Island, Indian Ocean, 22°S, 55°E) from 1 November 2014 to 31 October 2015, using wavelength-scanned cavity ring down spectroscopy. Except during cyclone periods where $\delta^{18}O_v$ is highly depleted (−20.5‰), a significant diurnal variability can be seen on both $\delta^{18}O_v$ and q_v with enriched (depleted) water vapor (mean $\delta^{18}O_v$ is −13.4‰ (−16.6‰)) and moist (dry) conditions (mean q_v is 9.7 g/kg (6.4 g/kg)) during daytime (nighttime). We show that $\delta^{18}O_v$ diurnal cycle arises from mixing processes for 65% of cases with two distinct sources of water vapor. We suggest that $\delta^{18}O_v$ diurnal cycle is controlled by an interplay of thermally driven land-sea breezes and upslope-downslope flows, bringing maritime air to the observatory during daytime, whereas at night, the observatory is above the atmospheric boundary layer and samples free tropospheric air. Interestingly, $\delta^{18}O_v$ record also shows that some nights (15%) are extremely depleted (mean $\delta^{18}O_v$ is −21.4‰). They are among the driest of the record (mean q_v is 2.9 g/kg). Based on different modeling studies, we suggest that extreme nocturnal isotopic depletions are caused by large-scale atmospheric transport and subsidence of dry air masses from the upper troposphere to the surface, induced by the subtropical westerly jet.

1. Introduction

Water vapor isotopic ratios ($\delta^{18}O_v$ and δD_v, hereafter δ_v) have been used for decades to explore atmospheric processes. The earliest studies provided measurements of the isotopic composition of near-surface vapor using cold trap and mass spectrometric techniques [*Jacob and Sonntag*, 1991; *Lawrence et al.*, 2004; *Lee et al.*, 2006; *Angert et al.*, 2008]. Tropospheric water vapor isotopic ratios have also been obtained from ground-based and spaceborne passive remote sensing techniques [*Frankenberg et al.*, 2009; *Herbin et al.*, 2009; *Worden et al.*, 2007; *Nassar et al.*, 2007; *Schneider et al.*, 2010; *Steinwagner et al.*, 2010]. They allow for isotopic measurements in total or partial columns. Recently, with the advent of commercial water vapor isotopic analyzers using cavity-enhanced spectroscopic methods [*Gupta et al.*, 2009], continuous time series coupling near-surface $\delta^{18}O_v$ and δD_v with specific humidity (q_v) have been obtained with a very high precision (<1‰ for δD_v) [e.g., *Tremoy et al.*, 2011; *Steen-Larsen et al.*, 2014] and a high frequency (<1 min).

All studies of the isotopic composition of water vapor have clearly revealed that monitoring pairing measurements of δ_v with q_v provides an additional value to our knowledge of atmospheric water budget, compared with measurements of water vapor mixing ratio alone. They have led to an improved understanding of many processes affecting atmospheric humidity, from polar to tropical regions, such as large-scale transport and mixing of air masses [*Noone et al.*, 2011, 2013; *Noone*, 2012; *Bailey et al.*, 2013, 2015; *Tremoy et al.*, 2012; *Steen-Larsen et al.*, 2015], convective organization and intensity [*Risi et al.*, 2008; *Tremoy et al.*, 2014; *Conroy*

et al., 2016], moistening processes such as evaporation of raindrops in lower troposphere [*Worden et al*., 2007; *Tremoy et al*., 2014], sublimation of ice or condensate detrainment in the upper troposphere [*Moyer et al*., 1996; *Kuang et al*., 2003; *Webster and Heymsfield*, 2003; *Nassar et al*., 2007; *Bony et al*., 2008; *Steinwagner et al*., 2010], clouds microphysics [*Samuels-Crow et al*., 2014], or dehydration processes induced by large-scale subsidence or equatorward transport from midlatitudes [*Galewsky et al*., 2007, 2011; *Galewsky and Hurley*, 2010; *Risi et al*., 2010a].

Water vapor in subtropical atmosphere plays a key role in the Earth's radiative budget [*Held and Soden*, 2000; *Pierrehumbert et al*., 2006]. Understanding processes that control the subtropical water budget, like moistening and dehydration, is crucial regarding the expected changes and their uncertainties in the subtropics in the context of climate change [*Seidel et al*., 2008]. In this context, several studies have recently used paired δ_v-q_v observations in subtropical regions to examine moisture transport and mixing in the troposphere (see *Galewsky et al*. [2016] for a recent review). Among these studies, isotopic measurements on stations located in a subtropical marine environment have provided new insights about the controls of the humidity of the atmospheric boundary layer (ABL) and the free troposphere. *Noone et al*. [2011], *Hurley et al*. [2012], and *Bailey et al*. [2013] on Mauna Loa, Hawaii (subtropical North Pacific), and *González et al*. [2016] in Tenerife, Canary Islands (subtropical North Atlantic), showed the relevance of water vapor exchange between the boundary layer and the free troposphere due to shallow convection at local scale. The later can transport boundary layer moisture across the trade wind inversion while entraining dry free tropospheric vapor into the boundary layer. In addition, *Bailey et al*. [2015] showed the importance to account for residual surface layers formed during previous mixing events to explain the isotopic composition of water vapor with simple mixing isotopic models. Subtropical humidity is also strongly affected by large-scale moisture transport and subsidence. Pairing measurements of humidity with isotopic observations have been used to detect extratropical moisture transport into the subtropics and to examine how important this transport is to influence moisture budget of the subtropical free troposphere [*Hurley et al*., 2012; *Bailey et al*., 2015; *González et al*., 2016].

However, studies based on isotopic observations and dealing with the variability of the subtropical atmospheric humidity, and its controls, in a marine environment in the Southern Hemisphere have not been reported, so far. Actually, as noted by *Galewsky et al*. [2016], there is an overrepresentation of studies dealing with the isotopic composition of water vapor in the Northern Hemisphere, whereas very few studies are conducted in the Southern Hemisphere and none in the Indian Ocean.

In order to fill this gap, we present and discuss here pairing measurements of humidity with isotopic observations obtained at Reunion Island, a French island located in the subtropical western part of the Indian Ocean, 700 km east of Madagascar (Figure 1). The mechanisms responsible for tropospheric moisture variability in this region can differ from previous ones pointed out in subtropical North Atlantic and Pacific. Moreover, the southwest Indian Ocean is somewhat poor in ground-based atmospheric observations. Our in situ measurements actively participate to the international effort to monitor atmospheric variables in this region [*Baray et al*., 2013], while a number of emerging activities related to climate change impacts are organized under the patronage of the Indian Ocean Commission at http://commissionoceanindien.org/. In particular, our isotopic observations will be very helpful to detect general circulation models biases in this region [*Risi et al*., 2012].

In our study, we explore the controls of subtropical humidity in the troposphere based on a 1 year long $\delta^{18}O_v$ and q_v data set in order to understand better the scheme of moisture exchange and transport. In addition to previous work done in Hawaii and Tenerife, we will also briefly discuss deuterium excess of water vapor defined as $d_v = \delta D_v - 8 \times \delta^{18}O_v$ [*Dansgaard*, 1964]. We aim at understanding how important mixing processes are to control humidity variability in the troposphere. Specifically, we aim at estimating the frequency of those mixing processes between the boundary layer and the free troposphere. We also examine how the subtropical jet may control extratropical transport during austral winter when it is nearest Reunion Island. We thus intend to discuss and to quantify the importance of local mixing processes and remote moisture transport for the control of the tropospheric humidity in a subtropical area where those questions have not been investigated yet. At last, we also discuss the interest to provide long-term monitoring of water vapor isotopic ratios at Reunion Island to track the different processes responsible for the expected changes in subtropical humidity in response to climate change.

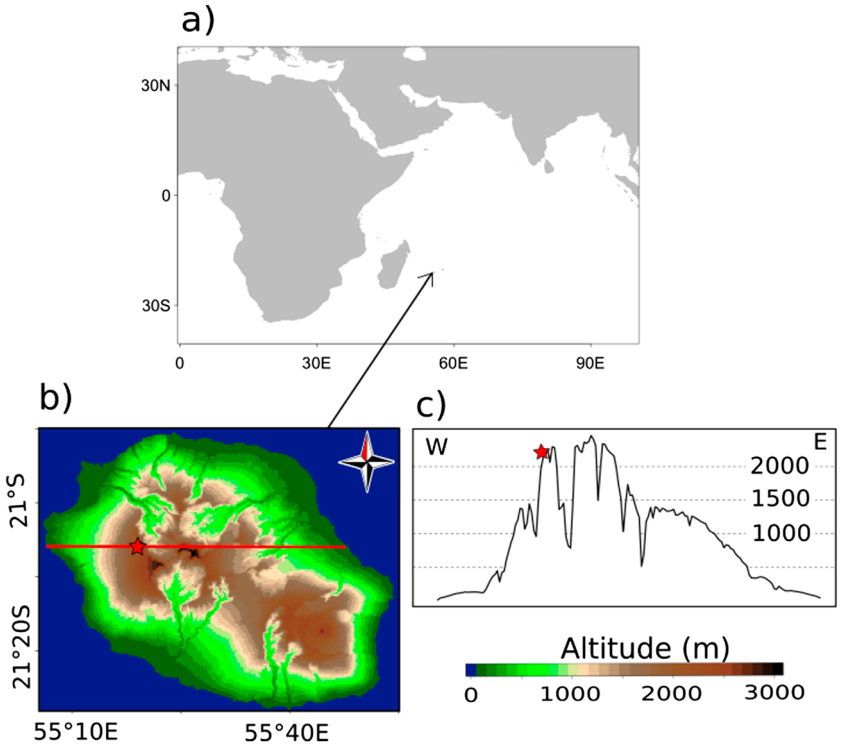

Figure 1. (a) Location of Reunion Island in the Indian Ocean, (b) topography of Reunion Island, and (c) west-east transect used in the MESO-NH simulation. The red star shows the location of the Maïdo observatory.

2. Data and Methods

2.1. The Maïdo Observatory

We have taken advantage of the facilities offered by the Maïdo observatory, an atmospheric platform dedicated to observations in the troposphere and stratosphere [*Baray et al*., 2013]. The Maïdo observatory (hereafter, MO) is located on a summit on the western side of Reunion Island (21.079°S, 55.383°E, 2160 m, Figure 1). The terrain of Reunion Island is dominated by two volcanic mountains, Piton des Neiges (~3070 m) and Piton de la Fournaise (~2630 m), both exceeding 2500 m in height, above the typical height of trade wind inversion (~2000 m). Thus, the northwestern and western parts of the island (the leeward side) are protected by the elevation from the prevailing easterly trade winds. In consequence, within a stable maritime environment with weak trade winds, the flow regime of the island is marked by land-sea breeze circulations and thermally driven diurnal winds, combining daytime sea breeze/upslope flow and nighttime land breeze/downslope flow [*Schroeder et al*., 1977; *Schroeder*, 1981; *Whiteman*, 1990; *Stull*, 1988; *Feng and Chen*, 1998]. As a result, during the day, air masses from the marine boundary layer are transported by upslope winds along the west coast toward the MO [*Lesouëf et al*., 2011]. When the daytime sea breeze weakens on the west coast, moist air masses can also originate from the nearby Cirque de Mafate (caldera east of Maïdo in Figure 1) or being advected from the windward (eastern) side of the island to Maïdo site by strong southeasterly trade winds [*Lesouëf*, 2010; *Lesouëf et al*., 2011, 2013; *Tulet et al*., 2017]. During the night, the transport pattern is reversed as trade wind flow is pushed offshore by divergence of cooled air from the land [*Baray et al*., 2013]. As the mixed layer collapses at sunset, the nocturnal boundary layer is typically below the altitude of the MO. As a consequence, we expect this site to be ideal to track mixing processes between the boundary layer and the free troposphere at the diurnal scale. In addition, Reunion Island is under the influence of large-scale tropical atmospheric circulation (Hadley cell and consequent subtropical subsidence and easterly winds, the presence of the Intertropical Convergence Zone far northward) and it also undergoes influences from midlatitude storm tracks, jet streams, and oceanic fronts [*Taupin et al*., 1999]. The MO site is thus expected to be also a good place to examine the influence of extratropical air incursion into the subtropical troposphere.

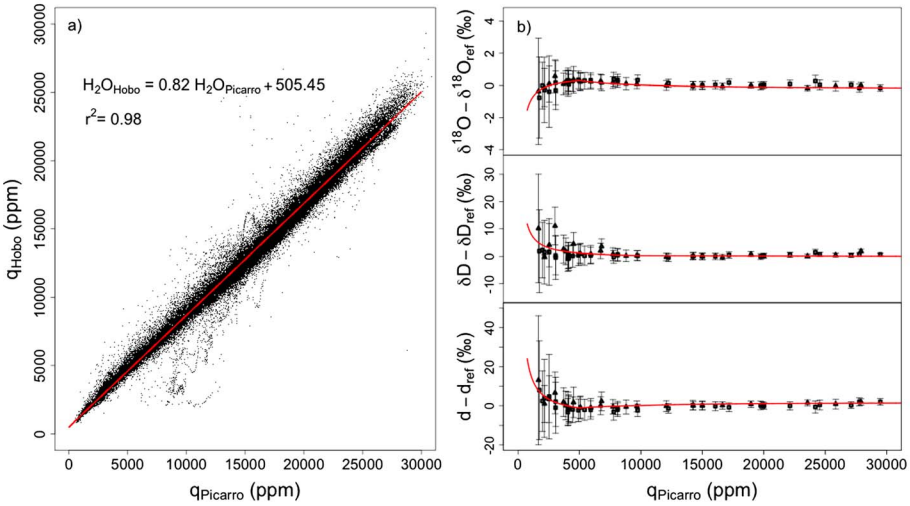

Figure 2. (a) Specific humidity of the Hobo sensor (q_{Hobo}, ppm) as a function of specific humidity measured by the Picarro ($q_{Picarro}$, ppm) from 1 November 2014 to 31 October 2015 (5 min averaged data). The linear regression is shown (red line, q_{Hobo} = 0.82 $q_{Picarro}$ + 505.45). (b) Isotopic dependence of the Picarro Inc. instrument on $q_{Picarro}$ for two different isotopic water standards along with one standard deviation (±1σ). The results are given as a deviation from the values at 15,000 ppm (named, δ_{ref} and d_{ref}). The first (second) standard was injected 32 (24) times at different humidity levels from 1738 (1669) to 32,590 (36,520) ppm.

2.2. Water Vapor Isotopic Measurements

Specific humidity (q_v) and the isotopic composition of water vapor (δ_v) have been measured at the MO from 1 November 2014 to 31 October 2015 by a Picarro Inc. instrument (L2130-i model), which is based on wavelength-scanned cavity ring down spectroscopy. The measurements have been made continuously except during periods of few days due to power failure or minor analyzer malfunctions. Our experimental setup is similar to the one described in *Tremoy et al.* [2011]. In short, water vapor is captured at 6.6 m above the surface (1.5 m above the roof of the MO) through a heated intake of 10 m long, 3/8 inch diameter tubing (perfluoroalkoxy). The sample line is pumped at ~0.6 L/min. As described in *Tremoy et al.* [2011], q_v was calibrated against relative humidity and temperature sensors (Hobos from Onset Computer Corp) over 12 months (Figure 2a). We also apply corrections to account for humidity dependence of the isotopic composition and for the instrumental isotopic drift following the protocol described in *Tremoy et al.* [2011]. Both corrections are determined using the Standard Module Delivery from Picarro Inc. The first correction was determined by injecting two water standards at different humidity levels from ~1600 to ~36,000 ppm (see Figure 2b and its legend). The isotopic calibration of the instrument is performed every 48 h based on the injection of two standards at a reference water vapor concentration of 20,000 ppm.

The short-term precision of the instrument (±1σ) during a 10 min stable measurement of water standard is better than ±0.2‰ and ±0.9‰ for $\delta^{18}O_v$ and δD_v, respectively, leading to a precision better than ±1.8‰ for deuterium excess. In the manuscript, we will only refer to $\delta^{18}O_v$ and d_v.

2.3. Models

In this section, we describe different modeling tools that will be used to discuss mixing processes between the marine boundary layer and the free troposphere and to examine large-scale moisture transport and subsidence. We present them in the next subsections.

2.3.1. The Isotopic Signature of Air Masses Mixing

The paired measurements of δ_v with q_v are used in this study to trace air masses mixing. In a δ_v-q_v diagram, mixing lines between two end-members (moisture sources) will trace hyperbolic curves [*Noone et al.*, 2011]. We consider that a marine air mass reservoir (marine end-member with q_m and δ_m as humidity and isotopic composition) is mixed with a free tropospheric air mass reservoir (free-tropospheric end-member with q_{Tropo} and δ_{Tropo} as humidity and isotopic composition) as time passes. In that case, the mass and the isotopic

balances between the two sources lead to a hyperbolic relationship between the isotopic composition (δ_v) of the mixing and its specific humidity (q_v) (our observations) which is described by the following equation:

$$\delta_v = q_{\text{Tropo}} \times \left[\delta_{\text{Tropo}} - \delta_m\right] \times \frac{1}{q_v} + \delta_m \quad (1)$$

2.3.2. The Isotopic Composition of the Ocean Evaporative Flux

In our discussion, we will investigate whether or not the daytime isotopic composition of water vapor at the MO site is consistent with a marine boundary layer origin and we will discuss our daytime observations relatively to the isotopic composition of the evaporative flux at the ocean surface (noted δ_{V0}). The later can be estimated following the model of *Merlivat and Jouzel* [1979]:

$$\delta_{V0} = \frac{1}{\alpha_{\text{eq}}} \times \frac{1-k}{1-kh} - 1 \quad (2)$$

where α_{eq} is the isotopic fractionation factor for oxygen 18 at equilibrium between liquid and vapor, h is the relative humidity of the atmosphere with respect to SST (sea surface temperature), and k is an empirical factor representing the wind regime over the ocean depending on the wind speed [*Merlivat and Jouzel*, 1979].

In order to estimate δ_{V0} above the Indian Ocean around Reunion Island, we used the European Centre for Medium-Range Weather Forecasts (ECMWF) Interim reanalysis data set [*Dee et al*., 2011] at 0.125° with a 6 h resolution for SST, h (at 2 m above sea level (asl)), and wind speed (at 10 m asl). Those three parameters were averaged over a small area surrounding Reunion Island: 54°–57°E, 20°–23°S (101,475 km^2).

2.3.3. Evolution of the ABL Diurnal Variability at the MO Site

While marine air is expected to reach the MO during the day because of the sea breeze/upslope transport, the MO site is expected to be in the free troposphere during the night as explained in section 2.1. However, no direct observation or measurement of the ABL height at the MO can confirm this assumption. We use a 24 h simulation (31 March to 1 April 2015) from the limited area research mesoscale model MESO-NH [*Lafore et al*., 1998] (http://mesonh.aero.obs-mip.fr/) to examine in detail the ABL evolution in the vicinity of the MO. Specifically, we examine vertical cross section of water vapor mixing ratio and squared Brunt-Väisälä frequency (N^2). The later is a proxy for maximum of vertical stability and is defined as follows in the atmosphere:

$$N^2 = \frac{g}{\theta}\frac{\mathrm{d}\theta}{\mathrm{d}z} \quad (3)$$

where θ is the potential temperature, z the altitude, and g the gravitational acceleration.

The simulation is done for a specific day with conditions representative of days outside cyclone periods (i.e., when the orographic and land-sea breeze regimes dominate).

Several MESO-NH simulations have been successfully performed over Reunion Island at different resolutions to study cyclone formation or pollutant transport [*Tulet and Villeneuve*, 2011; *Lesouëf et al*., 2011, 2013; *Jolivet et al*., 2013; *Durand et al*., 2014; *Sivia et al*., 2015; *Vérèmes et al*., 2016]. The model was set up with four two-way nested domains having horizontal grid spacing of 16, 8, 2, and 0.5 km and grid size of 200 × 200, 128 × 128, 128 × 128, and 192 × 160 points, respectively. Seventy vertical levels were used with the highest resolution near the surface (40 m) and the lowest at 27 km (600 m) (layer thickness increases of 7% up to 700 m and 8% above). The model was initialized on 29 March 2015 at 00:00 UTC. Initial and 6-hourly boundary conditions are provided by the operational ECMWF analyses [*European Centre for Medium-Range Weather Forecasts*, 2011]. The MO altitude in the model is ~1800 m.

2.3.4. Impact of Large-Scale Transport

To explore the relationship between the isotopic composition of water vapor and large-scale subsidence and to help determine the importance of extratropical transport in setting the free tropospheric end-member in our simple mixing isotopic model, we use two different models.

2.3.4.1. FLEXPART Simulations in May 2015 During the MORGANE Campaign

First, we will use the FLEXPART (FLEXible PARTicle dispersion model) Lagrangian particle dispersion model to assess air masses origin and transport pathways. We will focus on May 2015 to take advantage of the Maïdo ObservatoRy Gaz and Aerosols Ndacc Experiment (MORGANE) field campaign that started in May [*Duflot et al*., 2017]. Several meteorological radiosondes were launched from the MO during the campaign as part of an intercomparison exercise with the water vapor and ozone lidars. We used high vertical resolution profiles of temperature, relative humidity, and pressure measured by Vaisala RS92 radiosondes. This enables us to characterize in details the thermodynamic profile of the atmosphere above the MO during this period and to clearly identify nights during which the MO is above the ABL.

FLEXPART simulates the transport and dispersion of air masses by calculating the trajectory of a multitude of particles [*Stohl et al*., 2005]. The model is driven by operational ECMWF operational data with a temporal resolution of 1 h (analyses at 00:00 and 12:00 UTC are combined with hourly forecasts from 01:00 to 11:00 UTC and from 13:00 to 23:00 UTC) and a horizontal resolution of $1° \times 1°$ on 137 model levels. The vertical resolution decreases with altitude: it is about 20 m at the surface, 150 m at the top of the boundary layer (~2000 m), and up to 2500 m at around 75 km height.

For each FLEXPART simulation, 20,000 particles were released from the MO surface. The FLEXPART model simulations are run 10 days backward in time, and the position data of all particles every hour are used to define the centroid (or center of mass) of all particles [*Stohl et al*., 2002]. This technique reduces the results of the FLEXPART backward simulations to a condensed model output. This facilitates the analysis of the origin of the air masses by looking at a few trajectories associated with the centroids instead of analyzing each single back trajectory.

2.3.4.2. LMDZ-Iso Simulation From 1 November 2014 to 31 October 2015

Second, we will use the atmospheric general circulation models (AGCMs) ability to capture large-scale circulation to help evaluate the importance of extratropical transport and large-scale subsidence and their consequences on water vapor isotopic ratios at the surface but also on the vertical scale. We will use the AGCM LMDZ-iso, implemented with water stable isotopes [*Risi et al*., 2010b], with also a focus on May 2015.

LMDZ-iso resolution is 2.5° in latitude and 3.75° in longitude and offers here 27 vertical levels (from 1008 to 114 hPa). The vertical resolution is maximal at the surface (the first layer thickness is 72 m) and decreases with altitude (for example, the layer thickness including the MO is 443 m and increases to 882 m at 500 hPa). The simulated horizontal wind fields are nudged by those of the operational ECMWF analyses to ensure that the large-scale circulation is realistic on a day-to-day basis. It is worth noting that due to the coarse resolution of LMDZ-iso, Reunion Island is not represented in the model and the later can be used only to discuss impact of large-scale atmospheric circulation. As expected, $\delta^{18}O_v$ simulated in the first layer by LMDZ-iso is consistent with our calculations of $\delta^{18}O_{V0}$ (Table 2).

3. Results

3.1. The 1 Year Long $\delta^{18}O_v$ and q_v Variability

The $\delta^{18}O_v$ and q_v observations are presented in Figure 3. As expected, q_v shows a clear seasonal cycle with the highest (lowest) values (~12 g/kg) ($<$4 g/kg) occurring from December to January (July to September) during the wet (dry) season (Figure 3). By contrast, no seasonal cycle can be seen on $\delta^{18}O_v$ whose annual mean is -15.7 ± 3.4‰ (we give the mean $\pm 1\sigma$, here and throughout the manuscript) (Figure 3). However, we clearly detect on $\delta^{18}O_v$ strong isotopic depletions at the synoptic scale that are related to three tropical cyclone events in 2015: Bansi (from 8 to 19 January), Chedza (from 13 to 22 January), and Haliba (from March 5 to 12) systems ($\delta^{18}O_v$ is -20.5 ± 3.2‰, averaged over 23 days). It is worth noting that q_v does not exhibit any specific signal during those cyclone periods, pointing out here the added value of water stable isotopes. Although previous studies as *Lawrence and Gedzelman* [1996], *Lawrence et al*. [1998], *Scholl et al*. [2007], and *Fudeyasu et al*. [2008] have pointed out the potential of water stable isotopes for hurricane studies, this is beyond the scope of this paper and the specificity of our observations during those low-pressure systems will be addressed in a subsequent study.

As expected, our record shows quasi-permanent diurnal variations both in q_v and $\delta^{18}O_v$, except during the aforementioned tropical cyclone events. We characterize in details in the next section those diurnal cycles

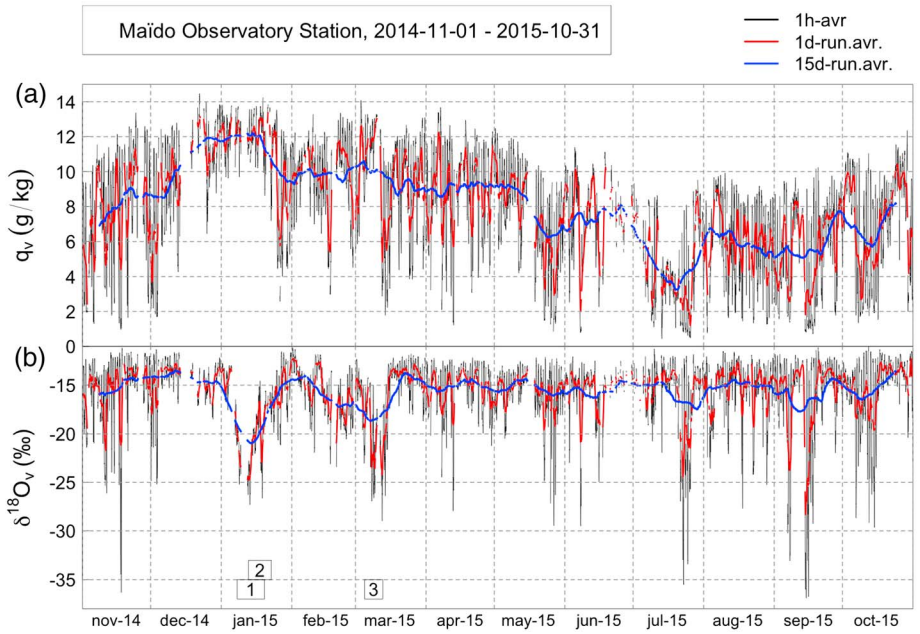

Figure 3. Time series from 1 November 2014 to 31 October 2015 of (a) specific humidity (q_v, g/kg) and (b) the isotopic composition (oxygen 18) of water vapor ($\delta^{18}O_v$, ‰) as measured by the Picarro Inc. instrument. Black, red, and blue lines refer to 1 h averaged data, 1 day, and 15 day running average data, respectively. The lack of data in q_v and δ_v corresponds to power interruptions or maintenance periods. The three hurricane events in 2015 are labeled with small rectangles as follows: 1-Bansi, 8–19 January; 2-Chedza, 13–22 January; and 3-Bansi, 5–12 March.

that are supposed to capture mixing processes between the ABL and the free troposphere due to local diurnal upslope-downslope flow.

3.2. The $\delta^{18}O_v$ Diurnal Cycle

During the day, $\delta^{18}O_v$ (q_v) attains a maximum and almost constant value between 11 A.M. and 5 P.M. LT (local time, UTC + 4) (mean $\delta^{18}O_v$ (q_v) is -13.4 ± 1.3‰ (9.7 ± 2.4 g/kg) over the whole period without accounting for the aforementioned cyclone periods), whereas at night both $\delta^{18}O_v$ and q_v exhibit minimum values between 11 P.M. and 5 A.M. LT (-16.6 ± 3.2‰ and 6.4 ± 2.9 g/kg, respectively). Daily (11 A.M.–5 P.M.) $\delta^{18}O_v$ values vary between -11.3 and -19.4‰, whereas at night (11 P.M.–5 A.M.) $\delta^{18}O_v$ values vary between -12.5 and -34.4‰, reaching for some nights very depleted values (without the aforementioned cyclonic periods). Regarding q_v, it varies from 1.9 and 14.0 g/kg in the 11 A.M.–5 P.M. time period and from 0.73 and 12.2 g/kg in the 11 P.M.–5 A.M. time period.

By further exploring nighttime, we are able to define extremely depleted and dry nights considering (1) the nights for which more than 75% of 5 min observations are available from 11 P.M. to 5 A.M. LT and (2) the nights exhibiting 5 min $\delta^{18}O_v$ values lower than the mean $\delta^{18}O_v$ minus 2σ (calculated over the whole 1 year record without tropical cyclone activity, i.e., $\delta^{18}O_v < -21.9$‰) between 11 P.M. and 5 A.M. LT. In this way, 52 extreme nights (relatively to classical nights) were identified out of 290 nights from 1 November 2014 to 31 October 2015 (i.e., 15.2%) with a mean $\delta^{18}O_v$ (q_v) between 11 P.M. and 5 A.M. of -21.4 ± 4.8‰ (2.9 ± 2.2 g/kg). The lowest 5 min isotopic values for those 52 nights are found sometimes before 11 P.M. or after 5 A.M. but always between 6 P.M. and 10 A.M.. Their mean δ_v and q_v values are -28.0 ± 4.7‰ and 1.70 ± 1.40 g/kg, respectively. Indeed, the use of the 11 P.M.–5 A.M. interval is less meaningful for extreme nights (compared to classical nights) which do not exhibit a flat isotopic level in the middle of the night (see Figure 4 for an example during May 2015). In comparison, mean $\delta^{18}O_v$ and q_v for classical nights are -16.0 ± 1.4 (-17.4 ± 1.8)‰ and 6.9 ± 1.9 (6.1 ± 2.1) g/kg, respectively, considering the 11 P.M.–5 A.M. period (the lowest 5 min isotopic values within 11 P.M.–5 A.M.). It is worth noting that (i) extreme nights are preferentially found during the dry austral winter season: 48% of them occur between June and September 2015 versus 6%

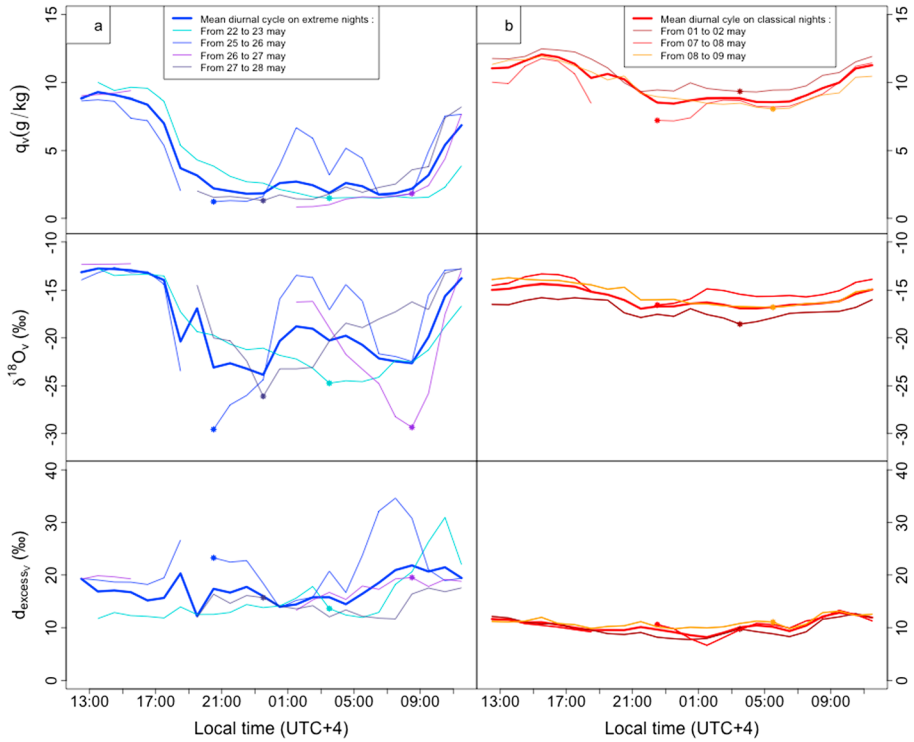

Figure 4. (a) Diurnal cycles of q_v (g/kg), $\delta^{18}O_v$ (‰), and d_v (‰) in May 2015 for each extreme nights (thin lines) and their mean (thick line). (b) Same for classical nights. Stars represent the hour of departure in FLEXPART model for the back-trajectories calculations (the most depleted hour in $\delta^{18}O_v$). Gaps are due to isotopic calibrations, except the gap of 26–27 May which is due to power issue.

between December 2014 and February 2015 and (ii) extreme nights tend to cluster over a 1 week period instead of being sporadically dispersed throughout the year.

4. Discussion About the Water Vapor Isotopic Ratios Diurnal Cycles

In this section, we first discuss the diurnal isotopic variations in terms of air masses mixing between a marine source reaching the MO during daytime and the free troposphere sampled at the MO at night (section 4.1). We use simple mixing isotopic models to determine how frequent mixing is and to characterize the moisture sources involved in mixing processes. In a second section, we focus on the extreme isotopic depleted nights defined in section 3. We examine whether atmospheric large-scale subsidence can explain such isotopic depletions and how important extratropical transport is in setting the free tropospheric source in mixing processes (section 4.2). At last, we compare the dynamical processes identified in Reunion Island to influence the tropospheric humidity with processes identified in other similar subtropical locations in Hawaii [*Noone et al*., 2011; *Bailey et al*., 2013, 2015] and Tenerife [*González et al*., 2016] (section 4.3).

4.1. Is Diurnal $\delta^{18}O_v$ Cycle Due To Air Masses Mixing?

4.1.1. Daytime Processes: Do Marine Air Masses Reach the MO?

The daytime MO water vapor ratio is remarkably stable year-round. In this section, we verify that the daytime isotopic composition of water vapor can be explained by arrival of water vapor originating from the surrounding ocean evaporation. To check this hypothesis, we compare our observations to the isotopic composition of the water vapor just above the Indian Ocean around La Reunion Island ($\delta^{18}O_{V0}$, calculated from equation (2); see section 2.3.2). $\delta^{18}O_{V0}$ exhibits a very weak and constant diurnal cycle all year long due to the small diurnal ECMWF Interim relative humidity variations (Figure 5). Over the whole record, the mean value of $\delta^{18}O_{V0}$ is -11.1 ± 0.6‰ and the mean amplitude of the diurnal $\delta^{18}O_{V0}$ cycle is 0.55 ± 0.08‰ (mean difference between the 11 A.M.–5 P.M. and 11 P.M.–5 A.M. stable periods). In consequence, the diurnal variations of $\delta^{18}O_v$ at the MO are not produced by any diurnal variation in $\delta^{18}O_{V0}$. However, we expect to sample

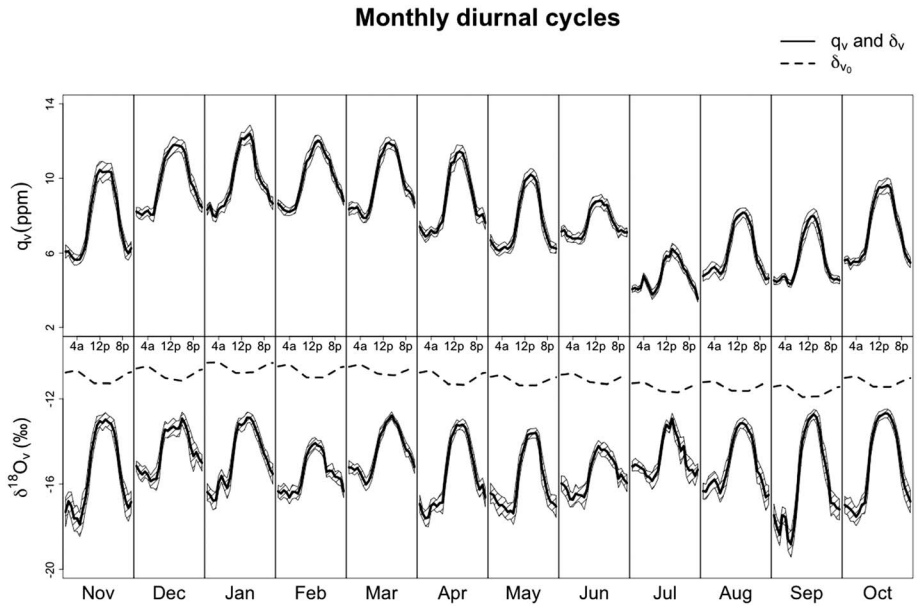

Figure 5. Monthly mean diurnal cycle for q_v (g/kg) and $\delta^{18}O_v$ (‰) as measured by the Picarro Inc. instrument (1 h data with one standard deviation, ($\pm 1\sigma$)) from November 2014 to October 2015 in local time (tick lines). The dashed lines correspond to $\delta^{18}O_{V0}$ (‰) which is the isotopic composition of water vapor formed by the ocean surface evaporation as calculated with the *Merlivat and Jouzel* [1979] model (see text).

marine air at the MO during the day because of the upslope and sea breeze flow regimes. Then, the day value of $\delta^{18}O_{V0}$ (-11.3‰ between 11 A.M. and 5 P.M.) has to be compared to our observations during daytime (-13.4‰). The observed $\delta^{18}O_v$ is -2.1‰ more depleted than $\delta^{18}O_{V0}$, leading to a mean isotopic gradient of -0.10‰/100 m for $\delta^{18}O_v$. This altitude gradient is in the expected range of isotopic gradients found in literature for tropical precipitation, especially in Reunion Island for which *Grunberger* [1989] found a gradient between -0.09 and -0.16‰/100 m from precipitation measurements. As the MO is 2160 m high, we attribute this isotopic difference to the entrainment mixing during convective boundary layer development drawing dry free tropospheric air into the boundary layer and lowering the water vapor isotope ratios close to the observatory [*Angert et al*., 2008; *Welp et al*., 2012; *Bailey et al*., 2013].

Thus, the isotopic values of water vapor during daytime at the MO are consistent with arrivals of marine vapor all year long. It likely originates from evaporation of the ocean west of the island before being transported to the MO by upslope flow. However, we cannot exclude that marine air masses are also transported to the MO from the windward side of the island. *Lesouëf et al*. [2011] showed in a high-resolution simulation that air masses measured near the surface at the MO could come from the east when a strong southeasterly trade wind regime dominates the flow over the island. However, the upslope regime along the west side of the island often dominates the flow at the MO and water vapor likely originates from the west.

Interestingly, it is worth noting that chemical species such as CO, O_3, and NO_x measured at the MO (in the framework of the international network GWA-Global Atmospheric Watching) that have anthropogenic ABL sources (urban and industrial activities in the northwestern part of the island) and, in consequence, that are supposed to be possible tracers of the ABL lack significant diurnal variations (A. Colomb, personal communication, 2017). While the isotopic composition of water vapor at the MO during the day is influenced by upslope transport from the marine boundary layer, other synoptic processes exert a control on the concentration of chemical tracers strong enough to offset the effect of sea breeze/upslope flow [see *Lesouëf et al*., 2011]. Therefore, water vapor isotopes appear to be the only adequate tracer of the ABL at the MO site.

4.1.2. Influence of the Free Troposphere at the MO During Nighttime

In the previous section, we showed that upslope transport of marine air masses controls the isotopic composition of water vapor at the MO during the day. The isotopic composition of water vapor at the MO is much lower at nighttime as well as humidity. This can reveal another moisture source that could be the free

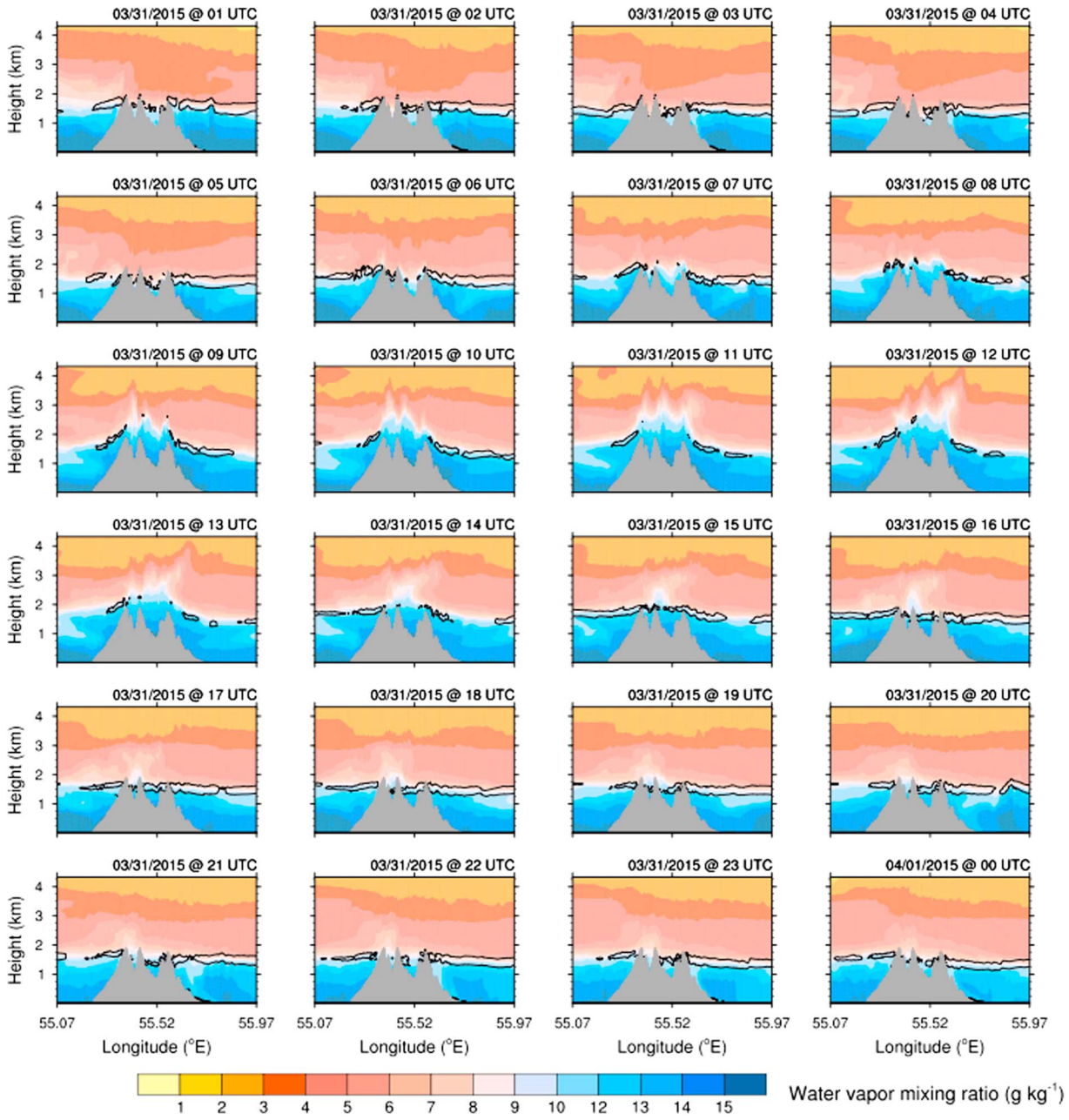

Figure 6. Vertical cross section of water vapor mixing ratio (g/kg) and square of the Brunt-Väisälä frequency (the black isoline is at 4.10^{-4} s^{-2}) along the west-east transect shown in Figure 1c between 31 March 2015 01:00 UTC and 1 April 2015 01:00 UTC as simulated by MESO-NH. The MO is the first summit on the left.

troposphere. In order to confirm that free tropospheric air can attain the MO at night, we now examine the diurnal variation of the ABL height at the MO site. Figure 6 shows hourly vertical cross sections of water vapor mixing ratio and squared Brunt-Väisälä frequency (N^2, see equation (3)) from MESO-NH simulation done on 31 March (section 2.3.3). The MO is located on the first western summit in Figure 6. Between 01:00 and 04:00 UTC (05:00 and 08:00 LT), high values of water vapor mixing ratio ($q_v > 15$ g/kg) are encountered below 800 m on the western side of the island, and there is a strong humidity gradient between 800 and 1800 m. The strong humidity gradient region coincides with the maximum values of N^2 (delimited by the black isoline at 4×10^{-4} s^{-2}), a proxy for maximum of vertical stability, which is found around 1500 m. Higher static stability is usually observed within the entrainment zone at the top of the ABL and beneath

the free troposphere, and thus, maximum values of static stability give an estimate of the ABL height. During the morning, thermally driven circulations develop and a sea breeze/upslope flow transports maritime air over the coastal areas along the western slope as depicted by high values of q_v (~13–14 g/kg) at 05:00 UTC. The sea breeze flow propagates further and supplies maritime water vapor to the MO. A wet layer with q_v values ~10–12 g/kg develops over the western mountain flank and attains a depth of ~1 km above the MO between 10:00 and 11:00 UTC. This demonstrates the vertical development of the ABL at the MO during the morning and early afternoon. The entrainment layer at the top of the ABL, as indicated by the maximum of the static stability, is displaced upward as the ABL develops. The early evening (14:00 UTC, 18:00 LT) corresponds to the onset of the downslope/land breeze flow and q_v values above the top of the mountains start to decrease. By 17:00 UTC (21:00 LT), the western summit is above the region of strong static stability and the surface water vapor mixing ratio (7–8 g/kg) has dropped by half compared to the daytime values (12–14 g/kg). Hence, the high-resolution Meso-NH simulation clearly indicates that for a representative day, the MO is immersed in the ABL during the day and is in the free troposphere at night. The Meso-NH simulation shows that the surface boundary conditions at the MO are produced by an interaction of the thermally driven local circulation with the free tropospheric flow. During the day, the upslope flow carries local, more humid air from the western coast to the MO, while during the night downslope flow brings air generally representative of the free troposphere to the observatory.

Thus, the depleted isotopic signature of δ_v during the night at the MO, coupled with lower specific humidity, can reflect water vapor originating from higher atmospheric levels in the free troposphere. This is consistent with expected isotopic composition of water vapor from higher altitude that are supposed to be more depleted as shown by several modeling studies and satellite observations [e.g., *Bony et al*., 2008] (see also section 4.2.2.4].

4.1.3. Evidence for Air Masses Mixing Between Marine and Free Tropospheric Sources

Our investigations done in sections 4.1.1 and 4.1.2 show that marine air mass reservoir (q_m and δ_m) is sampled at the MO around midday, while the free tropospheric air mass reservoir (q_{Tropo} and δ_{Tropo}) is sampled at the MO during the night. In time, one can assume that mixing occurs between those two reservoirs due to a competition between upslope and downslope transports. To check this hypothesis, we interpret our observations in a δ_v-q_v diagram (see section 2.3.1).

All 5 min $\delta^{18}O_v$ and q_v observations over 1 year are shown in Figure 7a. All the data follow a statistically hyperbolic fit (black curve, $r^2 = 0.50$, $p < 0.001$) except during hurricane events. The later are isolated in the right lower corner of the figure and exhibit a sharper decreasing of δ_v with q_v, consistent with what we expect for a pure Rayleigh or a super Rayleigh distillation as described by *Noone* [2012]. Considering the statistically hyperbolic fit as a potential mixing curve (see equation (1)), the isotopic composition of the moist end-member is −13.1‰. This value is lower by 1.8‰ than the isotopic composition of marine vapor formed during daytime (see section 4.1.1) and similar to the mean daytime $\delta^{18}O_v$ at the MO (see section 3).

To further discuss mixing processes, we distinguish classical and extreme nights in two δ_v-q_v diagrams (Figures 7b and 7c, respectively) and we exclude periods with tropical cyclones. In each diagram, we show two arbitrary mixing curves. They intercept one end-member that can correspond to the free troposphere (low values for q_v and δ_v) and another one that can correspond to the marine boundary layer (higher values for q_v and an isotopic composition slightly lower than δ_{V0}). Those mixing curves are determined to capture a maximum number of 5 min observations with end-members values calculated from our daytime and nighttime q_v and $\delta^{18}O_v$ observations as explained below.

Figure 7b corresponds to data recorded during the 52 extreme nights from 11 A.M. LT on the day corresponding to that night to 5 P.M. the following day. The higher mixing curve (light blue) depicts a mixing between a marine air with a composition of $q_v = 15$ g/kg (maximum observed values) and $\delta^{18}O_v = -12.1$‰ (mean daytime isotopic composition in the observations plus 1σ) (see section 3) and a free tropospheric end-member with a composition of $q_v = 0.3$ g/kg and $\delta^{18}O_v = -23.0$‰ (the driest 5 min data over the whole period). The second mixing curve (pink) depicts a mixing between a marine source similar to the previous one but with a $\delta^{18}O_v$ of −14.7‰ (mean daytime isotopic composition in the observations minus 1σ) and a free tropospheric end-member with a composition $q_v = 0.9$ g/kg and $\delta^{18}O_v = -40.0$‰ (the most depleted 5 min data over the whole period). Those two theoretical mixing curves include 77% of our observations.

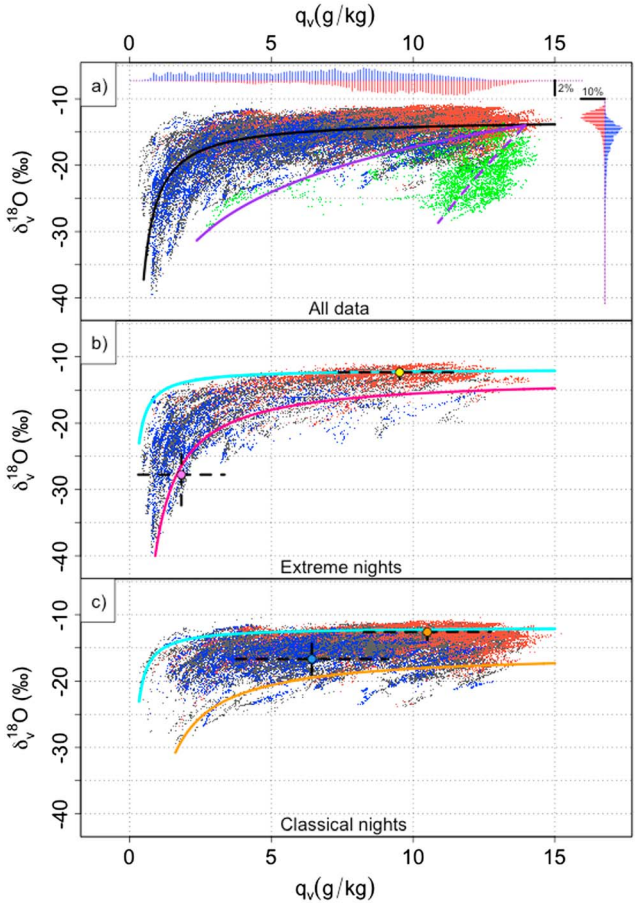

Figure 7. (a) The 5 min averaged $\delta^{18}O_v$ as a function of q_v from 1 November 2014 to 31 October 2015. Green dots represent all the cyclone periods (see text). Day (11 A.M.–5 P.M.) and night (11 P.M.–5 A.M.) data are in red and blue, respectively. Observations between day and night times are represented in grey. The distribution of 5 min $\delta^{18}O_v$ and q_v data is also shown for day and night times (red and blue bars, respectively) with a resolution of 0.25‰ and 0.1 g/kg, respectively. The statistically hyperbolic fit for the observations is plotted in black (it does not include cyclone periods). We also show for hurricane periods a pure Rayleigh (purple) and a super Rayleigh (dashed purple) distillation curves (T = 17.5°C, h = 86%, re-evaporation rate is 10%). (b) Same as Figure 7a without the cyclone periods but only for extreme nights and surrounding daytime (see text). Two theoretical mixing curves are represented (light blue, q_m = 15 g/kg, $\delta_m = -12.1$‰, q_{Tropo} = 0.3 g/kg, and $\delta_{Tropo} = -23.0$‰ and pink, q_m = 15 g/kg, $\delta_m = -14.7$‰, q_{Tropo} = 0.9 g/kg, and $\delta_{Tropo} = -40.0$‰). We also show the mean of the most depleted 5 min $\delta^{18}O_v$ for extreme nights (extended between 6 P.M. and 10 A.M.) (pink dot) and the mean of the most enriched 5 min $\delta^{18}O_v$ for days surrounding extreme nights (between 11 A.M. and 5 P.M.) (yellow dot). (c) Same as Figure 7b but for classical nights. A third theoretical mixing curve is shown (orange, q_m = 15 g/kg, $\delta_m = -17.3$‰, q_{Tropo} = 1.6 g/kg, and $\delta_{Tropo} = -30.8$‰). We also show the mean of the most depleted 5 min $\delta^{18}O_v$ for classical nights (between 11 P.M. and 5 A.M.) (blue dot) and the mean of the most enriched 5 min $\delta^{18}O_v$ for days surrounding classical nights (between 11 A.M. and 5 P.M.) (orange dot).

In Figure 7c, we plot observations recorded around the classical nights as done in Figure 7b for extreme nights. The light blue mixing curve is the same as in Figure 7b. It captures the more enriched observations as in Figure 7b. This is not surprising as daytime q_v and $\delta^{18}O_v$ values exhibit no difference whether or not the surrounding nights are extreme or classical nights. In order to capture the observations appearing in the lower left corner of the figure (depleted nights with middle- to high-humidity levels), we add a third arbitrary mixing curve (orange) with a marine end-member with a composition of q_v = 15 g/kg and $\delta^{18}O_v = -17.3$‰ (mean daytime isotopic composition in the observations minus 3σ) and a free tropospheric end-member with a composition of q_v = 1.6 g/kg and $\delta^{18}O_v = -30.8$‰ (the most depleted 5 min data over the whole period, excluding the extreme nights). This later mixing curve and the first one include 86% of our observations.

As the mixing is supposed to occur at the daily scale (from day to night and from night to day), we further explore the robustness of mixing in δ_v-q_v diagrams over 18 h periods (day to night: 11 A.M.–5 A.M. (day + 1) or night to day: 11 P.M.–5 P.M. (day + 1)) for which more than 75% of 5 min observations are available ($n > 162$). As prescribed in *Noone et al.* [2011], we determine that an 18 h period is controlled by mixing processes when data from that period can be characterized by a hyperbolic fit with a $r^2 > 0.8$ ($p < 0.001$). In this case, 93% of 18 h periods exhibit a mixing for extreme nights. In contrast, this percentage decreases to 59% when considering the 18 h classical periods. However, it is worth noting that Reunion Island is most of the time exposed to the lowest layers of the free troposphere. Indeed, in Figure 7c (classical nights), we only see a small section of the mixing gradient compared with Figure 7b (extreme nights). This limits the robustness of the hyperbolic fittings and may lower the estimation of mixing frequency for classical nights.

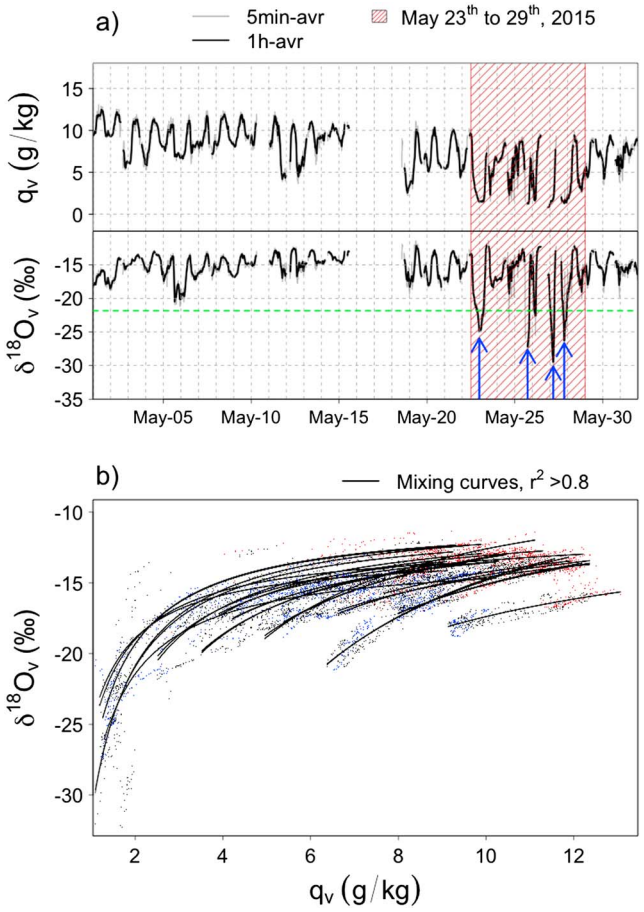

Figure 8. (a) q_v (g/kg) and $\delta^{18}O_v$ (‰) as in Figure 3 during May 2015 (interruptions (10, 15–18, and 26 May) are due to power issues). Other gaps, around 2 h, are due to isotopic calibration sequences. The green dashed line corresponds to the annual $\delta^{18}O_v$ mean (without cyclone periods) minus 2σ. Blue arrows show the four extreme nights. The red dashed period corresponds to extreme nights in LMDZ-iso (23 to 29 May 2015). (b) $\delta^{18}O_v$-q_v diagram. Small dots are 5 min averaged data as in Figure 7. Black curves represent the hyperbolic fit from day to night or night to day when $r^2 > 0.8$.

4.1.4. Summary

As a conclusion, we show that our diurnal δ_v and q_v observations are well described by mixing between marine and free tropospheric sources, except during hurricanes when observations are described by Rayleigh or super Rayleigh processes. Whereas the marine end-member is stable, the free tropospheric end-member differs between classical and extreme nights. We further explore in the next section the role of large-scale subsidence in setting the free tropospheric end-member.

4.2. Focus on Nocturnal Extreme Isotopic Depletions

To better explore the variability of the isotopic composition during nights and especially the atmospheric mechanisms leading to extreme isotopic depletion for 15% of them, we focus our discussion on May 2015 for which independent observations obtained during the MORGANE campaign confirm that the MO is most of the time above the ABL at night (section 4.2.1). Then, we explore how extratropical moisture transport and large-scale subsidence can explain the extremely depleted δ_v in May 2015 over Reunion Island (section 4.2.2).

4.2.1. Analysis of Nighttime Periods During the MORGANE Campaign in May 2015

A total of 18 radiosondes were launched during the MORGANE campaign (see section 2.3.4.1): 8 during the day between 1 P.M. and 4 P.M. LT and 10 at night between 8 P.M. and 12 A.M. LT. Based on both equivalent potential temperature (Θ_e) and relative humidity profiles, daily radio soundings clearly show that the MO is within the ABL (not shown). Six nighttime profiles of Θ_e (11–12, 12–13, 18–19, 22–23, 26–27, and 28–29) clearly show a stable atmosphere indicating that the MO is in the free troposphere (see Figure S1 in the supporting information). Three nighttime profiles of Θ_e (7–8, 15–16, and 19–20) show rather constant value above the MO, and the relative humidity profiles depict values between 50 and 75% that could be associated with isolated humid layers potentially altering the Θ_e profiles (see Figure S1). This assumption is supported by the fact that Meteosat infrared satellite pictures at the closest hour of these night radio soundings show cloudy sky (not shown). At last, for the 21–22 night, Θ_e profile decreases until ~2700 m (as well as the relative humidity) (see Figure S1) indicating the presence of an unstable layer up to this altitude. Θ_e profile then increases above 2700 m, and the humid layers above 4000 m can be also associated to cloudy layers according to Meteosat pictures. Thus, those nighttime Θ_e and relative humidity profiles tend to confirm that the MO is most of the nighttime above the ABL in May 2015 and that a residual surface layer can be maintained for some nights nonetheless.

During May 2015, we have identified on our observations four extreme nights following the definition of an extreme night given in section 3 (see arrows in Figure 8a): one night from 22 to 23 May and three nights from 25 to 28 May. Those extreme nights have a mean signature (11 P.M.–5 A.M.) of 2.3 ± 1.7 g/kg and −20.3 ± 4.1‰ for q_v and $\delta^{18}O_v$, respectively, while the other nights have a mean signature of 7.0 ± 1.9 g/kg and −17.5 ± 1.6‰ for q_v and $\delta^{18}O_v$, respectively. The mean of the lowest 5 min isotopic composition (q_v) for the four extreme nights is −29.2 ± 3.5‰ (1.4 ± 0.3 g/kg) and is observed between 6 P.M. and 10 A.M. We note that for two of those extreme nights we have radio soundings that clearly indicate that the MO is in the free troposphere (no radiosounding is available for the 25–26 and 27–28 May nights).

As in section 4.1.3, we examine our observations in a δ_v-q_v diagram (Figure 8b) to ensure that mixing processes occur during this period. We determine that 53% of the 18 h periods in May 2015 are controlled by mixing processes (the four extreme nights and surrounding daytime observations are included).

4.2.2. Influence of the Subtropical Jet and Induced Large-Scale Subsidence on δ_v

4.2.2.1. The Be^7 Observations

First, it is worth noting that the presence of large-scale subsidence occurring at the end of May 2015 is supported by independent daily measurements of the Be^7 concentration at Sainte-Suzanne in Reunion Island, in the northeast of the island (P. Heinrich, personal communication, 2017). Be^7 can be a proxy of large-scale subsidence: it is produced in the stratosphere with a half-life of 52.8 days preventing the particles to reach the surface in normal conditions [*Dorman*, 2004]. However, during periods of intensification of large-scale subsidence, the Be^7 concentration at the surface increases [*Feely et al*., 1989]. This is what we observe on 25–29 May 2015 (not shown).

4.2.2.2. Subtropical Jet Position in May 2015 and Associated Large-Scale Subsidence

A prominent feature of the upper tropospheric circulation in the Southern Hemisphere is the subtropical westerly jet that is stronger during the austral winter season (May to September). Figure 9a shows the average wind speed at 200 hPa for May 2015 as well as the 500 hPa vertical velocity in pressure coordinate (omega in units of hPa/d). At 200 hPa, the jet is discontinuous with a jet streak at 25°S from about 80°E to about 120°W and a jet streak near 40°S south of Africa. We then compare large-scale vertical motions (uplifts or subsidence) in the atmosphere for classical versus extreme nights. The vertical velocity at 500 hPa is used to indicate rising (negative omega values) or subsiding (positive omega values) air masses in the vicinity of Reunion Island. We then average daily omega values over the dates corresponding to classical and extreme nights. A strong contrast in the omega values exists around Reunion Island between classical (Figure 9b) and extreme periods (Figure 9c). During classical nights, regions of rising motions prevail near 30°S with omega peaking at −100 hPa/d. Classical nights also correspond to an absence of the jet over the Western Indian Ocean and an eastward shift of the jet over Australia. In contrast, during extreme nights a distinct region of increased subsidence is observed south of Reunion Island and is associated with the westward displaced jet stream over the Indian Ocean. During extreme nights, the entrance region (i.e., region upstream from wind speed maximum in the jet stream) of the subtropical jet is east of the island. In the entrance region, at high levels, air is accelerating due to the flow confluence. This acceleration generates ageostrophic wind from the north in the Southern Hemisphere, creating divergent and convergent zones on the northern and southern side of the jet streak, respectively. The convergence on the southern side of the jet streak results in downward motion of air in the right entrance region.

Interestingly, Figure 9c exhibits a wavelike structure in the 500 hPa omega field east of Madagascar spreading from the Western Indian Ocean to Australia between 20° and 30°S. The evolution of this pattern after approximately 21 May seems to indicate eastward propagation across the Indian Ocean and is linked to the jet activity over the Indian Ocean/Australia. A similar wavelike pattern can be found in the meridional wind field at ~200 hPa (not shown). Rossby waves can produce large-scale meridional movement of air and strong westerly jets can act as Rossby waveguides, i.e., focusing and trapping perturbations. In addition, *Hoskins and Karoly* [1981] indicate that the upper troposphere is the most important region for Rossby wave propagation in the tropical and subtropical regions. We thus suggest that the wavelike structure observed at the end of May 2015 may be a synoptic Rossby wave train in the upper troposphere. To further highlight the wave propagation and evolution, additional analysis of dynamical fields (e.g., horizontal winds and potential vorticity) would be required. However, the direct relationship between Rossby wave activity and variability in the upper level wind field over the Indian Ocean is beyond the scope of the present study.

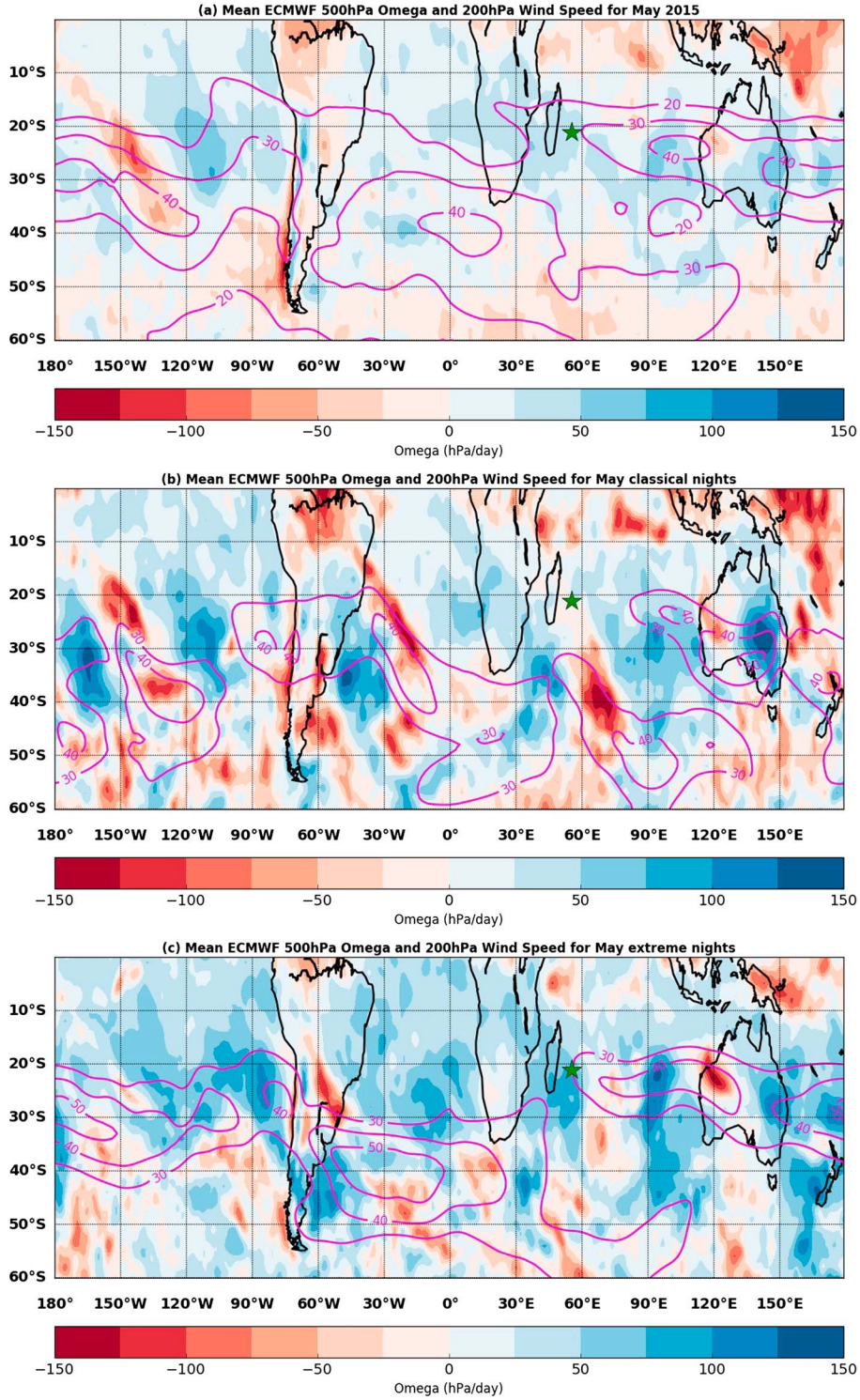

Figure 9. (a) Monthly mean wind speed (m/s) at 200 hPa and monthly mean pressure vertical velocity (omega in hPa/d) at 500 hPa for May 2015. (b) Mean omega at 500 hPa and wind speed at 200 hPa for periods corresponding to classical nights in May 2015 (1–2, 7–8, and 8–9 May) and (c) Same as Figure 9b for extreme nights (22–23, 25–26, 26–27, and 27–28 May). On each figure the isotachs (in magenta) are labeled and contoured every 10 m/s. The data are from operational ECMWF data at a resolution of 1° × 1°. The position of Reunion Island is indicated by a green star on each figure.

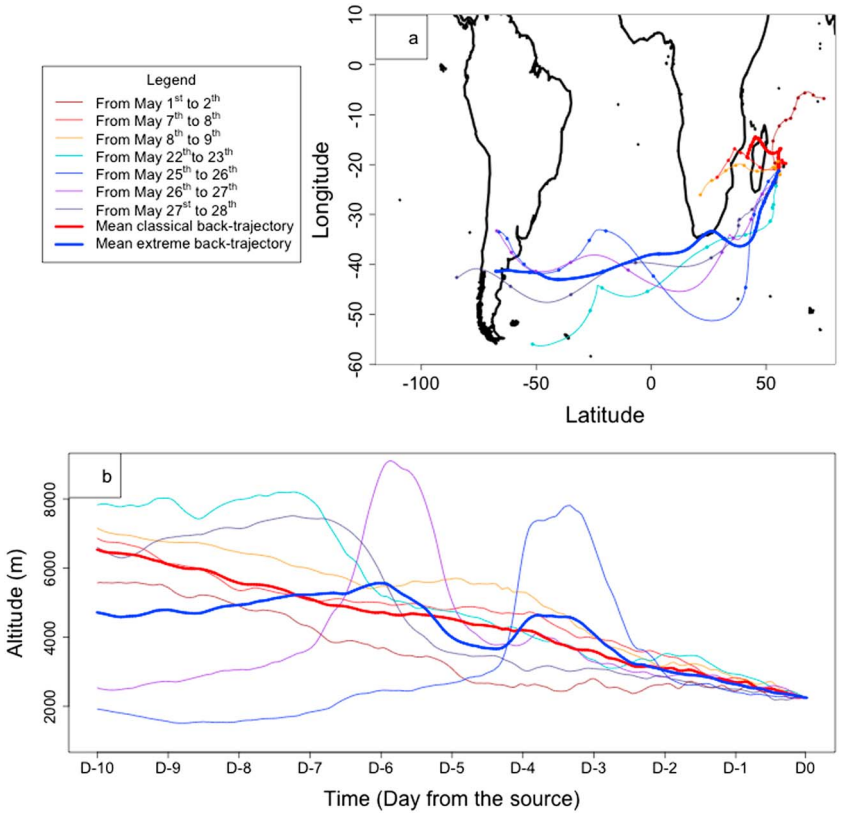

Figure 10. (a) The 10 day back trajectories computed with the FLEXPART Lagrangian model for extreme and classical nights. The mean back trajectories for classical nights (red thick line) and extreme nights (blue thick line) are also indicated. They are temporal means (mean position at day-1, day-2, and so on). Initial release times of the trajectories from the MO surface are indicated in Figure 4 (stars) and summarized in Table 1. Dots along back trajectories show the air parcel position every 24 h. (b) Evolution of the altitude of air parcels along each back trajectory (thin lines), also reported in Table 1. The mean air parcel altitude for classical and extreme nights is also shown in red and blue, respectively (tick line).

As a conclusion of this subsection, the location of the jet, east of the island, during extreme nights in May 2015, favors increased subsidence over the island and transport of air from the upper troposphere to the surface.

4.2.2.3. Moisture Sources and Air Masses Trajectories

Here we compare air mass transport pathways for three classical nights in May 2015 with the four extreme nights described above (we selected only three classical nights representative to limit the number of FLEXPART simulations). We selected classical nights following three criteria: (1) at least one night for which a radio sounding is available and shows that the MO is in the free troposphere as a reference case, (2) nights with continuous isotopic data or limited gaps in the measurements, and (3) nights for which the difference between daytime and nighttime isotopic mean values is as small as possible. Thus, nights on 1–2, 7–8, and 8–9 May 2015 were selected as classical nights. In particular, the night on 7–8 May was chosen because there is a radio sounding at 8 P.M. LT clearly showing that the MO is in the free troposphere although an isotopic calibration on the Picarro instrument leads to a gap in the data at the start of the night. The δ_v and q_v diurnal cycles for those four extreme and three classical nights can be seen in Figures 4a and 4b, respectively.

Figure 10a shows the 10 day FLEXPART back trajectories of the centroids of particles released from the MO surface for periods corresponding to isotopic minima during classical and extreme nights (indicated by stars in Figure 4). The FLEXPART simulations clearly show that air mass transport pathways are completely different for classical and extreme nights. For classical nights, air masses originate from the Indian Ocean or from South Africa, and transport pathways are no longer than 3900 km over 10 days. In contrast, the FLEXPART back trajectories indicate that air masses measured during extreme nights experienced long-range transport from

Table 1. Mean Altitude (m) of Air Parcels Every 24 h Along the 10 Days Long Back Trajectories Calculated With the FLEXPART Model for the Selected Classical (1–2, 7–8, and 8–9) and Extreme (22–23, 25–26, 26–27, and 27–28) Nights During May 2015[a]

	May 2015 Classical Nights			May 2015 Extreme Nights			
Date (DT, UTC)	1 (23:30)	7 (18:30)	9 (01:30)	22 (23:30)	25 (17:30)	27 (04:30)	27 (19:30)
$\delta^{18}O_v$ (‰)	−18.6	−16.6	−16.8	−24.9	−27.2	−29.5	−26.3
Mean (‰)		−17.3			−27.0		
q_v (g/kg)	9.3	7.2	8.1	1.5	1.3	1.8	1.3
Mean (g/kg)		8.2			5.9		
Days (24 h) from DT							
From 0 to −1	2438	2463	2591	2615	2311	2527	2325
From −1 to −2	2600	3086	3125	3314	2630	2868	2641
From −2 to −3	2550	3733	3563	3267	4467	3073	2939
From −3 to −4	2580	4337	4714	3805	7396	3803	3086
From −4 to −5	2706	4787	5523	4471	3334	4067	3414
From −5 to −6	3457	4912	5568	4937	2526	7980	4388
From −6 to −7	3914	5053	5686	6613	2159	5595	7018
From −7 to −8	4675	5298	6247	8112	1665	3282	7369
From −8 to −9	5173	5860	6662	7725	1537	2882	7018
From −9 to −10	5559	6591	6921	7856	1751	2571	6516

[a] $\delta^{18}O_v$ (‰) and q_v (g/kg) are also given for each night at the hour corresponding to the departure time (DT) at the MO for back-trajectory calculations, as well as an average for classical and extreme nights. Departure time (DT) is the nocturnal hour for which water vapor isotopic ratio is the most depleted at day 0 (in brackets, UTC time, see also stars in Figure 4).

the southern part of South America over the Atlantic Ocean and subsequent subsidence over Reunion Island, following the subtropical jet dynamic. Air masses traveled a mean distance of around 15,000 km in 10 days. The wavelike patterns in the trajectories for those extreme nights indicate that air parcels followed the subtropical jet dynamic.

We also examine the variations in altitude of the air masses represented by the FLEXPART back trajectories (Figure 10b). The daily altitudes for each trajectory are reported in Table 1. The air parcels altitude profiles for the three classical nights are similar, i.e., a linear decreased altitude along the pathway from 5560–6920 m, suggesting a slow and continuous subsidence over the course of the air masses history (420 m per day in average). Altitude variations of air parcels for the four extreme nights are highly different. For 22–23 and 27–28 May nights, air masses travel in the high troposphere before day-6 and start subsiding at day-5 south of South Africa/Madagascar which is consistent with the effects of the jet and the subsidence. For the two other nights (25–26 and 26–27), air parcels travel at low altitude at the beginning and attain the high troposphere (7400 and 8000 m, respectively) where they stay for about 1 day. Then, they leave the subtropical jet at around day-4 and day-2, respectively, before attaining the MO. This pathway, combining alternative low and high altitudes, could be explained by an atmospheric wave at 45°S which is visible in omega anomalies in Figure 9c. Thus, the extreme isotopic depletion during those four nights could arise from a long-range transport associated with the jet dynamic that brings higher-altitude dryer and depleted air to the MO surface. The isotopic depletion can be caused by an important air masses isotopic distillation, a reduced water vapor recharge from the surface due to high travel altitude and a higher-altitude/latitude transport in colder conditions.

The upper tropospheric origin of water vapor during the four extreme nights is also supported by deuterium excess and specific humidity. From 22–23 to 27–28 May deuterium excess show values up to 40‰ during night (Figure 4a), compared with a mean of 11.5 ± 3.1‰ (from 11 P.M. to 5 A.M.) and values within a 5.1‰–34.1‰ range for classical nights in May 2015 (see also deuterium excess for the three classical nights in Figure 4b). This second-order parameter is difficult to interpret in this subtropical region. However, high deuterium excess could be associated with subsidence of air from the upper troposphere as expected from vertical 1-D and cloud-resolving models implemented with water stable isotopes [*Bony et al.*, 2008; *Blossey et al.*, 2010] and from the atmospheric general circulation models LMDZ-iso (see below). At last, extreme nights at the end of May 2015 show a very low specific humidity of 1.5 ± 0.2 g/kg compared with a mean value of 6.3 ± 2.0 g/kg for the other nights in May 2015 (averages here are calculated over the most

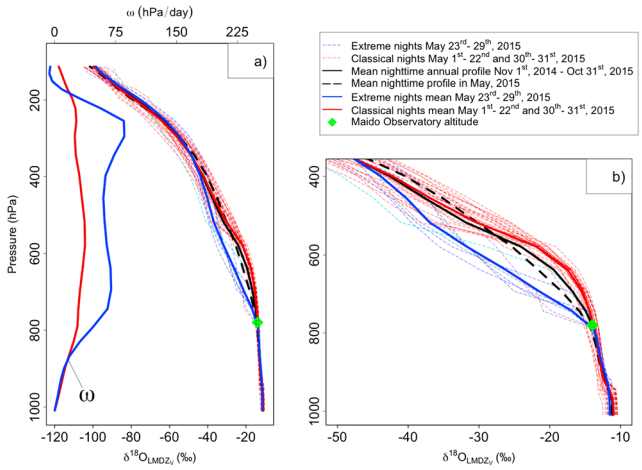

Figure 11. (a and b) LMDZ-iso $\delta^{18}O_v$ vertical profiles (‰). The vertical velocity (ω, in hPa/d) is also shown in Figure 11a. Outputs are given at 00:30 UTC for each day. Profiles refer to the grid including Reunion Island. Thick black profiles correspond to the mean from 1 November 2014 to 31 October 2015. Dashed black profiles refer to May 2015 mean profile. Thin red (blue) profiles refer to LMDZ-iso classical (LMDZ-iso extreme) nights from 1 to 22 and 30 to 31 May 2015 (from 23 to 29 May 2015). We also show the corresponding May 2015 mean profiles (thick red and blue profiles). The green diamond represents the MO altitude.

depleted 1 h $\delta^{18}O_v$ and so they are slightly different from values given in section 4.2.1). Those low specific humidity values are consistent with a high-altitude origin of water vapor.

4.2.2.4. Large-Scale Atmospheric Circulation in LMDZ-Iso in May 2015

Finally, we explore the ability of LMDZ-iso to reproduce extreme nights at the end of May 2015. Then, we discuss the link between those extreme depleted nights and large-scale subsidence based on the simulated vertical profiles of both water vapor isotopic ratios and vertical velocity (ω) that are expected to be different for classical and extreme nights.

As expected, LMDZ-iso shows stronger subsidence in the troposphere, between 195 and 867 hPa, at 00:30 UTC from May 23 to 29 (time period including the four extreme nights in our observations in May 2015 as highlighted in Figure 8) compared with other nights in May 2015 although the difference in ω is lower than 100 hPa/d (see mean ω profiles in Figure 11a for 23–29 May nights and the other nights of May).

As a consequence, LMDZ-iso simulates more depleted isotopic composition at 00:30 UTC for 23–29 May nights (hereafter, LMDZ-iso extreme nights) than during the other nights of May (hereafter, LMDZ-iso classical nights) within the atmospheric layers above the Maïdo altitude (see Table 2 and Figures 11a and 11b). The model simulates a significant depletion in the isotopic vertical profiles for LMDZ-iso extreme nights between 790 and 342 hPa (Figure 11b). The mean isotopic composition in this layer is −31.1 ± 12.1‰ (compared with −26.8 ± 12.8‰ considering the LMDZ-iso classical nights). A maximum difference (Figure 11b) of −9.3‰ is found between 637 and 578 hPa considering the LMDZ-iso extreme and classical nights isotopic mean profiles. It is worth noting also that vertical profiles of deuterium excess simulated by LMDZ-iso for May 2015 confirm increased values of d_v with altitude above 578 hPa (not shown). Mean deuterium excess from surface to 578 hPa is 12.0 ± 0.3‰ with no vertical gradient. Above 578 hPa, d_v increases at a rate of ~8‰/100 hPa until ~200 hPa and then around 75‰/100 hPa up to 114 hPa (not shown). We also observe

Table 2. Mean (±1σ) Isotopic Composition of Water Vapor ($\delta^{18}O_v$, ‰) in May 2015 at 00:30 UTC (00:04 A.M. LT) for the Whole Month, the Classical and the Extreme Nights for Observations at the Maïdo Observatory, $\delta^{18}O_{V0}$ (Calculation From *Merlivat and Jouzel* [1979]) (see text), and in LMDZ-Iso for Different Atmospheric Layers[a]

$\delta^{18}O_v$ (‰)	May 2015 00:30 UTC	May 2015 Classical Nights 00:30 UTC	May 2015 Extreme Nights 00:30 UTC
Maïdo δ_v (~790 hPa)	−16.9 ± 2.4	−16.3 ± 1.4	−19.9 ± 4.4
Ocean surface (δ_{V0})	−10.9 ± 0.5	-	-
LMDZ-iso 1008 hPa	−11.1 ± 0.6	-	-
LMDZ-iso 790 hPa	−13.7 ± 0.5	−13.8 ± 0.5	−13.8 ± 0.4
LMDZ-iso 744 hPa	−14.9 ± 1.7	−14.4 ± 0.7	−16.8 ± 2.6
LMDZ-iso 693 hPa	−16.8 ± 3.0	−15.5 ± 0.8	−21.5 ± 3.2

[a]Extreme nights in LMDZ-iso are recorded from 23 to 29 May. Extreme and classical nighttime isotopic values at 00:30 UTC in LMDZ-iso only differ above the 790 hPa level and are not mentioned below this layer.

that vertical profiles for LMDZ-iso extreme nights show higher deuterium excess in water vapor from the surface to 578 hPa by 3.3 ± 0.8‰ (the mean surface d_v value for LMDZ-iso extreme night is higher by 4.3‰) (not shown).

So LMDZ-iso well captures the large-scale subsidence at the end of May 2015 and their impact on both δ_v and d_v, at the surface but also on the vertical scale. This clearly supports our interpretation linking large-scale subsidence and extreme depleted isotopic values during some nights, as well as the added value of deuterium excess measurements to examine such processes.

4.2.2.5. Summary

In conclusion of this section, we demonstrate that the free tropospheric end-member of mixing process is sensitive to large-scale subsidence, which is controlled by the subtropical jet dynamics. Therefore, nighttime δ_v and d_v can be seen as tracers of the subtropical jet position relative to Reunion Island. The repartition of extreme nights over our 1 year long record supports this assumption as most of them are recorded during austral winter (see section 3) when the subtropical jet is close to Reunion Island. In the meantime, air masses that are transported by the subtropical jet have different origins (Atlantic and South America versus eastern Africa/Indian Ocean). Therefore, these differences in air masses origin and history could also contribute to the isotopic composition variations observed in our measurements.

4.3. How Reunion Island Results Compared With Other Similar Locations?

This section is a comparative discussion of previous studies dealing with isotopic observations in subtropical marine environments in regard to our study: what lessons can be drawn?

The strong common finding between our study and previous ones at Mauna Loa observatory in Hawaii [*Noone et al*., 2011] and on Tenerife Island [*González et al*., 2016] is the capacity of pairing δ_v measurements with q_v to capture mixing processes at the diurnal scale between the ABL and the free troposphere although upslope flow dynamic can vary from the windward to the leeward side of island [*Bailey et al*., 2015].

Our nighttime δ_v observations at Reunion Island provide also additional insights on extratropical moisture transport when Reunion lies under a jet entrance. Based on an Eulerian and a Lagrangian last saturation model, *Hurley et al*. [2012] demonstrated the importance of accounting for extratropical transport to explain paired isotopic observations over a few weeks in Hawaii. *Bailey et al*. [2015] confirmed the importance of the jet position in determining the isotope ratios at that site based on longer observations. *González et al*. [2016] led to a similar conclusion correlating back trajectories to isotopes ratios. In addition to previous work, our observations at Reunion Island suggest that nighttime deuterium excess might be a stronger tracer of such moisture remote transport as it exhibits very high values during extreme nights when extratropical transport dominates. Therefore, special efforts should be made in all studies to calibrate carefully laser spectrometers in order to provide reliable deuterium excess values.

Our study also confirms that water vapor isotopic ratios are much more robust in tracing the ABL diurnal variability compared with chemical or aerosol tracers as already pointed out by *Bailey et al*. [2015]. *González et al*. [2016] showed also that water stable isotopes provide new insights in addition to dust measurement into the influence of the African continent on the moisture budget of subtropical North Atlantic.

As a conclusion of this comparative section, the studies on Hawaii, Tenerife, and Reunion islands lead to very similar conclusions about the controls of the humidity in the subtropical troposphere. Mixing processes and large-scale subsidence exert a control strong enough on subtropical humidity to explain most of water vapor isotopic ratios variability although atmospheric processes characterizing each location can play an occasional role (as the dust outbreaks over the subtropical North Atlantic or the hurricane events at Reunion Island during the austral summer).

A major and common lesson from those studies is that high-altitude stations in the free subtropical troposphere in both hemispheres are key locations to study moisture exchange and transport. Long-term monitoring of both $\delta^{18}O_v$ and δD_v will thus offer information to investigate moistening and dehydration processes in subtropical troposphere (in opposite to diurnal q_v variations alone) and their changes in a context of climate change. Indeed, other tracer studies have shown that the frequency of extratropical transport to subtropics is sensitive to climate variability [*Lin et al*., 2014].

5. Conclusion

In this paper, we present a 1 year long time series of the isotopic composition of near-surface water vapor isotopic and of specific humidity at the Maïdo observatory (2160 m asl) in Reunion Island.

Our observations show the influence of the free troposphere and the ABL air on δ_v at night (depletion) and during the day (enrichment), respectively. The δ_v diurnal variations are controlled by an interplay of thermally driven land-sea breezes and upslope-downslope flows and reflects the immersion of the Maïdo site in the ABL during the day, whereas at night the site is located above the ABL, leading to a depletion of δ_v. This is supported by Meso-NH simulation of the ABL evolution in the vicinity of the observatory for a day in March 2015 with typical flow patterns for this time of the year (i.e., weak trade wind flow over the island and diurnal island-induced flow on the slopes of the island) and also by LMDZ-iso simulation of vertical profiles of water vapor isotopic ratios, showing isotopic depletion increasing with altitude consistent with our observations. Analysis of the observations in a δ_v-q_v diagram confirms that the water vapor isotopic ratio diurnal cycle at the Maïdo site is well described by mixing processes for 59% of the data, increasing to 93% when considering only periods of extreme nocturnal isotopic depletion.

Indeed, our observations exhibit a large range of isotopic depletions at night, with some extreme isotopic depletion for 15% of nights. Based on May 2015 observations as an initial exploration, we suggest here that the extreme nocturnal depletions are caused by large-scale atmospheric transport and subsidence over Reunion Island induced by the subtropical jet. The FLEXPART simulations show that air parcels sampled during extreme nights originate from southern part of South America and travel over the Atlantic Ocean to Reunion Island before subsiding toward Reunion Island from 2 to 6 days before attaining the Maïdo surface. For classical nights, the source is located in the Indian Ocean or in South Africa and air masses travel mostly in the lower troposphere.

Thus, we show that δ_v in Reunion Island can be used to trace mixing processes between the ABL and the free troposphere. It also records extratropical transport and subsidence bringing upper troposphere air to the surface. We suggest that deuterium excess in water vapor can be a better tracer of the large-scale subsidence. The investigations done with LMDZ-iso also suggest that large-scale subsidence could be further examined from vertical observations of the isotopic composition of water vapor.

However, our interpretation on the links between variations in large-scale subsidence, long-range transport, and strong isotopic depletion at night is mostly based on nights in May 2015. We will need to extend our analysis to other months in 2015 (July and September capture the most depleted nights) and in 2016 and 2017 to reinforce our conclusions. In addition, the study of longer series of δ_v and q_v will also enables us to further explore the hurricane events signal, characterized by a strong depletion of water vapor with a complete disappearance of diurnal cycles and so mixing processes.

Thus, general climate conclusions cannot be drawn yet from this relatively short-term record. But our study demonstrates that mountain sites, such as the Maïdo observatory, can provide a unique window for continuous long-term isotopic observations in the subtropical Southern Hemisphere where there is a relative lack of observations. More generally, this study and the previous ones, carried out in subtropical environments, show that long-term observations of water isotopic ratios might provide important insights in understanding future changes in subtropical water cycle, specifically the extratropical moisture transport and its frequency evolution.

Acknowledgments

This study was supported by Institut de Recherche pour le Développement, Commissariat à l'énergie atomique et aux énergies alternatives, CNRS-INSU, and by the ANR proposal 12-BS06-001. The authors acknowledge OPAR (Observatoire de Physique de l'Atmosphère à La Réunion), funded by CNRS- INSU and Université de La Réunion and managed by OSU-R (Observatoire des Sciences de l'Univers à La Réunion, UMS 3365). Meso-NH simulation was performed using computer resources allocated by GENCI (project 6660). We deeply thank B. Minster at LSCE for the analyses of all water isotopic standards. We also deeply thank an anonymous reviewer and Adriana Bailey for their very constructive comments, improving the manuscript and especially the scientific discussion. All data may be obtained from E. Guilpart (etienne.guilpart@lsce.ipsl.fr) or F. Vimeux (francoise.vimeux@lsce.ipsl.fr).

References

Angert, A., J.-E. Lee, and D. Yakir (2008), Seasonal variations in the isotopic composition of near-surface water vapour in the eastern Mediterranean, *Tellus*, *60B*, 674–684.

Bailey, A., D. Toohey, and D. Noone (2013), Characterizing moisture exchange between the Hawaiian convective boundary layer and free troposphere using stable isotopes in water, *J. Geophys. Res. Atmos.*, *118*, 8208–8221, doi:10.1002/jgrd.50639.

Bailey, A., J. Nusbaumer, and D. Noone (2015), Precipitation efficiency derived from isotopes ratios in water vapor distinguishes dynamical and microphysical influences on subtropical atmospheric constituents, *J. Geophys. Res. Atmos.*, *120*, 9119–9137, doi:10.1002/2015JD023403.

Baray, J. L., et al. (2013), Maïdo observatory: A new high-altitude station facility at Reunion Island (21°S, 55°E) for long-term atmospheric remote sensing and in situ measurements, *Atmos. Meas. Tech.*, *6*, 2865–2877, doi:10.5194/amt-6-2865.

Blossey, P. N., Z. Kuang, and D. M. Romps (2010), Isotopic composition of water in the tropical tropopause layer in cloud-resolving simulations of an idealized tropical circulation, *J. Geophys. Res.*, *115*, D24309, doi:10.1029/2010JD014554.

Bony, S., C. Risi, and F. Vimeux (2008), Influence of convective processes on the isotopic composition ($\delta^{18}O$ and δD) of precipitation and water vapor in the tropics: Part 1. Radiative-convective equilibrium and TOGA-COARE simulations, *J. Geophys. Res.*, *113*, D19305, doi:10.1029/2008JD009942.

Conroy, J. L., D. Noone, K. M. Cobb, J. W. Moerman, and B. L. Konecky (2016), Paired stable isotopologues in precipitation and vapor: A case study of the amount effect within western tropical Pacific storms, *J. Geophys. Res. Atmos.*, *121*, 3290–3303, doi:10.1002/2015JD023844.

Dansgaard, W. (1964), Stable isotopes in precipitation, *Tellus*, *16*, 436–468.

Dee, D. P., S. M. Uppala, A. J. Simmons, P. Berrisford, and P. Poli (2011), The ERA-interim reanalysis: Configuration and performance of the data assimilation system, *R. Meteorol. Soc.*, *137*, 553–597.

Dorman, L. (2004), *Cosmic Rays in the Earth's Atmosphere and Underground*, 862 pp., Springer, Netherlands, Kluwer Acad., Dordrecht, Netherlands, doi:10.1007/978-1-4020-2113-8.

Duflot, V., et al. (2017), Ozone profiles by DIAL at Maïdo observatory (Reunion Island) part 1. Tropospheric ozone lidar: System description, performances evaluation and comparison with ancillary data, *Atmos. Meas. Tech. Discuss.*, doi:10.5194/amt-2016-403.

Durand, J., P. Tulet, M. Leriche, S. Bielli, N. Villeneuve, A. Di Muro, and J.-B. Fillipi (2014), Modeling the lava heat flux during severe effusive volcanic eruption: An important impact on surface air quality, *J. Geophys. Res. Atmos.*, *119*, 11,729–11,742, doi:10.1002/2014JD022034.

European Centre for Medium-Range Weather Forecasts (2011), ECMWF's operational model analysis, starting in 2011, Research Data Archive at the National Center for Atmospheric Research, Computational and Information Systems Laboratory, doi:10.5065/D6ZG6Q9F.

Feely, H. W., R. J. Larsen, and C. G. Sanderson (1989), Factors that cause seasonal variations in beryllium-7 concentration in surface air, *J. Envrion. Radioactivity*, *9*, 223–249.

Feng, J., and Y. L. Chen (1998), Evolution of katabatic flow on the islanfd of Hawaï during 10 August 1990, *Mon. Weather Rev.*, *126*, 2185–2199.

Frankenberg, C., et al. (2009), Dynamic processes governing lower-tropospheric HDO/H_2O ratios as observed from space and ground, *Science*, *325*, 1374–1377.

Fudeyasu, H., K. Ichiyanagi, A. Sugimoto, K. Yoshimura, A. Ueta, M. D. Yamanaka, and K. Ozawa (2008), Isotope ratios of precipitation and water vapor observed in Typhoon Shanshan, *J. Geophys. Res.*, *113*, D12113, doi:10.1029/2007JD009313.

Galewsky, J., M. Strong, and Z. D. Sharp (2007), Measurements of water vapor D/H ratios from Mauna Kea, Hawaii, and implications for subtropical humidity dynamics, *Geophys. Res. Lett.*, *34*, L22808, doi:10.1029/2007GL031330.

Galewsky, J., and J. V. Hurley (2010), An advection-condensation model for subtropical water vapor isotopic ratios, *J. Geophys. Res.*, *115*, D16116, doi:10.1029/2009JD013651.

Galewsky, J., C. Rella, Z. Sharp, K. Samuels, and D. Ward (2011), Surface measurements of upper tropospheric water vapor isotopic composition on the Chajnantor Plateau, Chile, *Geophys. Res. Lett.*, *38*, L17803, doi:10.1029/2011GL048557.

Galewsky, J., H. C. Steen-Larsen, R. D. Field, J. Worden, C. Risi, and M. Schneider (2016), Stable isotopes in atmospheric water vapor and applications to the hydrologic cycle, *Rev. Geophys.*, *54*, 809–865, doi:10.1002/2015RG000512.

González, Y., et al. (2016), Detecting moisture transport pathways to the subtropical North Atlantic free troposphere using paired H_2O-δD in situ measurements, *Atmos. Chem. Phys.*, *16*, 4251–4269, doi:10.5194/acp-16-4251.

Grunberger, O. (1989), Etude géochimique et isotopique de l'infiltration sous climat tropical constrasté,massif du Piton des neiges, île de La Réunion, PhD, p. 280, Univ. of Paris XI, Paris.

Gupta, P., D. Noone, J. Galewsky, C. Sweeney, and B. H. Vaughn (2009), Demonstration of high-precision continuous measurements of water vapor isotopologues in laboratory and remote field deployment using wavelength-scanned cavity ring-down spectroscopy (WS-CRDS) technology, *Rapid Commun. Mass Spectrom.*, *23*, 2534–2542, doi:10.1002/rcm.4100.

Held, I., and B. Soden (2000), Water vapor feedback and global warming, *Annu. Rev. Energy Environ.*, *25*, 441–475.

Herbin, H., D. Hurtmans, C. Clerbaux, L. Clarisse, and P. F. Coheur (2009), (H_2O)-O-16 and HDO measurements with IASI/MetOp, *Atmos. Chem. Phys.*, *9*, 9433–9447.

Hoskins, B. J., and D. Karoly (1981), The steady linear response of a spherical atmosphere to thermal and orographic forcing, *J. Atm. Sciences*, *38*, 1179–1196.

Hurley, J. V., J. Galewsky, J. Worden, and D. Noone (2012), A test of the advection-condensation model for subtropical water vapor using stable isotopologue observations from Mauna Loa observatory, Hawaii, *J. Geophys. Res.*, *117*, D19118, doi:10.1029/2012JD018029.

Jacob, H., and C. Sonntag (1991), An 8-year record of the seasonal variation of ^2H and ^{18}O in atmospheric water vapor and precipitation at Heildelberg, Germany, *Tellus*, *43B*, 291–300.

Jolivet, S., F. Chane-Ming, D. Barbary, and F. Roux (2013), A numerical study of orographic forcing on TC Dina (2002) in South West Indian Ocean, *Ann. Geophys.*, *31*, 107–125.

Kuang, Z., G. C. Toon, P. O. Wennberg, and Y. L. Yung (2003), Measured HDO/H_2O ratios across the tropical tropopause, *Geophys. Res. Lett.*, *30*(7), 1372), doi:10.1029/2003GL017023.

Lafore, J. P., et al. (1998), The MESO-NH atmospheric simulation system. Part I: Adiabatic formulation and control simulations, *Ann. Geophys.*, *16*, 90–109.

Lawrence, J. R., and S. D. Gedzelman (1996), Low stable isotope ratios of tropical cyclone rains, *Geophys. Res. Lett.*, *23*, 527–530.

Lawrence, J. R., S. D. Gedzelman, X. P. Zhang, and R. Arnold (1998), Stable isotope ratios of rain and vapor in 1995 hurricanes, *J. Geophys. Res.*, *103*, 11,381–11,400, doi:10.1029/97JD03627.

Lawrence, J. R., S. D. Gedzelman, D. Dexheimer, H. K. Cho, G. D. Carrie, R. Gasparini, C. R. Anderson, K. P. Bowman, and M. I. Biggerstaff (2004), Stable isotopic composition of water vapor in the tropics, *J. Geophys. Res.*, *109*, D06115, doi:10.1029/2003JD004046.

Lee, X., R. Smith, and J. Williams (2006), Water vapour $^{18}O/^{16}O$ isotope ratio in surface air in New England, USA (2005), *Tellus*, *58B*, 293–304.

Lesouëf, D. (2010), Étude numérique des circulations locales à La Réunion: application à la dispersion de polluants, PhD thesis, 204 pp., Université de La Réunion, https://tel.archives-ouvertes.fr/tel-00633096.

Lesouëf, D., F. Gheusi, R. Delmas, and J. Escobar (2011), Numerical simulations of local circulations and pollution transport over Reunion Island, *Ann. Geophys.*, *29*, 53–69.

Lesouëf, D., F. Gheusi, P. Chazette, R. Delmas, and J. Sanak (2013), Low tropospheric layers over Reunion Island in Lidar-derived observations and a high-resolution model, *Boundary Layer Meteorol.*, *149*, 425–453, doi:10.1007/s10546-013-9851-9.

Lin, M., L. W. Horowitz, S. J. Oltmans, A. M. Fiore, and S. Fan (2014), Tropospheric ozone trends at Mauna Loa observatory tied to decadal climate variability, *Nat. Geosci.*, *7*, 136–143, doi:10.1038/ngeo2066.

Merlivat, L., and J. Jouzel (1979), Global climatic interpretation of the deuterium-oxygen 18 relationship for precipitation, *J. Geophys. Res.*, *84*, 5029–5033, doi:10.1029/JC084iC08p05029.

Moyer, E. J., F. W. Irion, Y. L. Yung, and M. R. Gunson (1996), ATMOS stratospheric deuterated water and implications for troposphere-stratosphere transport, *Geophys. Res. Lett.*, *23*, 2385–2388.

Nassar, R., P. F. Bernath, C. D. Boone, A. Gettelman, S. D. McLeod, and C. P. Rinsland (2007), Variability in HDO/H2O abundance ratios in the tropical tropopause layer, *J. Geophys. Res.*, *112*, D21305, doi:10.1029/2007JD008417.

Noone, D. (2012), Pairing measurements of the water vapor isotope ratio with humidity to deduce atmospheric moistening and dehydration in the tropical mid-troposphere, *J. Clim.*, *25*(13), 4476–4494.

Noone, D., et al. (2011), Properties of air mass mixing and humidity in the subtropics from measurements of the D/H isotope ratio of water vapor at the Mauna Loa observatory, *J. Geophys. Res.*, *116*, D22113, doi:10.1029/2011JD015773.

Noone, D., et al. (2013), Determining water sources in the boundary layer from tall tower profiles of water vapor and surface water isotope ratios after a snowstorm in Colorado, *Atmos. Chem. Phys.*, *13*, 1607–1623, doi:10.5194/acp-13-1607-2013.

Pierrehumbert, R., H. Brogniez, and R. Roca (2006), On the relative humidity of the atmosphere, in *The Global Circulation of the Atmosphere*, pp. 143–185, Princeton Univ. Press, Princeton, N. J.

Risi, C., S. Bony, F. Vimeux, L. Descroix, B. Ibrahim, E. Lebreton, I. Mamadou, and B. Sultan (2008), What controls the isotopic composition of the African monsoon precipitation? Insights from event-based precipitation collected during the 2006 AMMA field campaign, *Geophys. Res. Lett.*, *35*, L24808, doi:10.1029/2008GL035920.

Risi, C., S. Bony, F. Vimeux, C. Frankenberg, D. Noone, and J. Worden (2010a), Understanding the Sahelian water budget through the isotopic composition of water vapor and precipitation, *J. Geophys. Res.*, *115*, D24110, doi:10.1029/2010JD014690.

Risi, C., S. Bony, F. Vimeux, and J. Jouzel (2010b), Water-stable isotopes in the LMDZ4 general circulation model: Model evaluation for present-day and past climates and applications to climatic interpretations of tropical isotopic records, *J. Geophys. Res.*, *115*, D12118, doi:10.1029/2009JD013255.

Risi, C., et al. (2012), Process-evaluation of tropospheric humidity simulated by general circulation models using water vapor isotopic observations: 2. Using isotopic diagnostics to understand the mid and upper tropospheric moist bias in the tropics and subtropics, *J. Geophys. Res.*, *117*, D05304, doi:10.1029/2011JD016623.

Samuels-Crow, K. E., J. Galewsky, Z. Sharp, and K. J. Denis (2014), Deuterium excess in subtropical free troposphere water vapor: Continuous measurements from the Chajnantor Plateau, *Geophys. Res. Lett.*, *41*, 8652–8659, doi:10.1002/2014GL062302.

Schneider, M., K. Yoshimura, F. Hase, and T. Blumenstock (2010), The ground-based FTI network's potential for investigating the atmospheric water cycle, *Atmos. Chem. Phys.*, *10*, 3427–3442.

Scholl, M. A., T. W. Giambelluca, S. B. Gingerich, M. A. Nullet, and L. L. Loope (2007), Cloud water in windward and leeward mountain forests: The stable isotope signature of orographic cloud water, *Water Resour. Res.*, *43*, W12411, doi:10.1029/2007WR006011.

Schroeder, T. A. (1981), Characteristics of local winds in Northwest Hawaii, *J. Appl. Meteorol.*, *20*, 874–881.

Schroeder, T. A., B. J. Kilonsky, and B. N. Meisner (1977), Diurnal variations in rainfalla nd cloudiness, UHMET report 77–03, Department of Meteorologyn Univ. of Hawaï, 67 pp.

Seidel, D. J., Q. Fu, W. J. Randel, and T. J. Reichler (2008), Widening of the tropical belt in a changing climate, *Nat. Geosci.*, *1*, 21–24, doi:10.1038/ngeo.2007.38.

Sivia, S. G., F. Gheusi, C. Mari, and A. Di Muro (2015), Simulations and parameterisation of shallow volcanic plumes of Piton de la Fournaise, Réunion Island using Méso-NH version 4-9-3, *Geosci. Model Dev.*, *8*, 1427–1443.

Steen-Larsen, H. C., A. E. Sveinbjornsdottir, A. J. Peters, V. Masson-Delmotte, M. P. Guishard, G. Hsiao, J. Jouzel, D. Noone, J. K. Warren, and J. W. C. White (2014), Climatic controls on water vapor deuterium excess in the marine boundary layer of the North Atlantic on 500 days of in situ, continuous measurements, *Atmos. Chem. Phys.*, *14*, 7741–7756, doi:10.5194/acp-14-7741-2014.

Steen-Larsen, H. C., A. E. Sveinbjornsdottir, T. Jonsson, F. Ritter, J. L. Bonne, V. Masson-Delmotte, H. Sodemann, T. Blunier, D. Dahl-Jensen, and B. M. Vinther (2015), Moisture sources and synoptic to seasonal variability of North Atlantic water vapor isotopic composition, *J. Geophys. Res. Atmos.*, *120*, 5757–5774, doi:10.1002/2015JD023234.

Steinwagner, J., S. Fueglistale, G. Stiller, T. von Clarmann, M. Kiefer, P. P. Borsboom, A. van Delden, and T. Rockmann (2010), Tropical dehydration processes constrained by the seasonality of stratospheric deuterated water, *Nat. Geosci.*, *3*, 262–266.

Stohl, A., S. Eckhardt, C. Forster, P. James, N. Spichtinger, and P. Seibert (2002), A replacement for simple back trajectory calculations in the interpretation of atmospheric trace substance measurements, *Atmos. Environ.*, *36*(29), 4635–4648.

Stohl, A., C. Forster, A. Frank, P. Seibert, and G. Wotawa (2005), Technical note: The Lagrangian particle dispersion model FLEXPART version 6.2, *Atmos. Chem. Phys.*, *5*, 2461–2474, doi:10.5194/acp-5-2461-2005.

Stull, R. (1988), *An Introduction to Boundary Layer Meteorology*, vol. 13, pp. 10–30, Springer, Dordrecht, Netherlands.

Taupin, F. G., M. Bessafi, S. Baldy, and P. J. Bremaud (1999), Tropospheric ozone above the southwestern Indian Ocean is strongly linked to dynamical conditions prevailing in the tropics, *J. Geophys. Res.*, *104*, 8057–8066.

Tremoy, G., F. Vimeux, O. Cattani, S. Mayaki, I. Souley, and G. Favreau (2011), Measurements of water vapor isotope ratios with wavelength-scanned cavity ring-down spectroscopy technology: New insights and important caveats for deuterium excess measurements in tropical areas in comparison with isotope-ratio mass spectrometry, *Rapid Commun. Mass Spectrom.*, *25*, 3469–3480, doi:10.1002/rcm.5252.

Tremoy, G., F. Vimeux, S. Mayaki, I. Souley, O. Cattani, C. Risi, G. Favreau, and M. Oi (2012), A 1-year long δ^{18}Orecord of water vapor in Niamey (Niger) reveals insightful atmospheric processes at different timescales, *Geophys. Res. Lett.*, *39*, L08805, doi:10.1029/2012GL051298.

Tremoy, G., F. Vimeux, S. Soumana, I. Souley, C. Risi, G. Favreau, and M. Oï (2014), Clustering mesoscale convective systems with laser-based water vapor δ^{18}O monitoring in Niamey (Niger), *J. Geophys. Res. Atmos.*, *119*, 5079–5013, doi:10.1002/2013JD020968.

Tulet, P., and N. Villeneuve (2011), Large scale modeling of the transport, chemical transformation and mass budget of the sulfur emitted during the eruption of April 2007 by the Piton de la Fournaise, *Atmos. Chem. Phys.*, *11*, 4533–4546.

Tulet, P., et al. (2017), First results of the Piton de la Fournaise STRAP 2015 experiment: Multidisciplinary tracking of a volcanic gas and aerosol plume, *Atmos. Chem. Phys.*, *17*, 5355–5878, doi:10.5194/acp-17-5355-2017.

Vérèmes, H., J.-P. Cammas, J.-L. Baray, P. Keckhut, C. Barthe, F. Posny, P. Tulet, D. Dionisi, and S. Bielli (2016), Multiple subtropical stratospheric intrusions over Reunion Island: Observational, Lagrangian and Eulerian numerical modeling approaches, *J. Geophys. Res. Atmos.*, *121*, 14,414–14,432, doi:10.1002/2016JD025330.

Webster, C. R., and A. J. Heymsfield (2003), Water isotope ratios D/H, ^{18}O/^{16}O, ^{17}O/^{16}O in and out of clouds map dehydration pathways, *Science*, *302*(5651), 1742–1745.

Welp, L. R., X. Lee, T. J. Griffis, X.-F. Wen, W. Xiao, S. Li, X. Sun, Z. Hu, M. Val Martin, and J. Huang (2012), A meta-analysis of water vapor deuterium excess in the midlatitude atmospheric surface layer, *Global Biogeochem. Cycles*, *26*, GB3021, doi:10.1029/2011GB004246.

Whiteman, C. D. (1990), Observations of thermally developped wind system sis mountainous terrain, Chapter 2 in Atmospheric processes over complex terrain (W. Blumen, Ed), Meteorological Monographs, 23, n°45. American Mateorological Society, Boston, Massachusetts, 5–42.

Worden, J., D. Noone, K. Bowman, and the Tropospheric Emission Spectrometer science team & data contributors (2007), Importance of rain evaporation and continental convection in the tropical water cycle, *Nature*, *445*, 528–532, doi:10.1038/nature05508.